Loss of insulin signaling may contribute to atrial fibrillation and atrial electrical remodeling in type 1 diabetes

Iuliia Polina[a,1], Hailey J. Jansen[a,b,c,1], Tiesong Li[a], Motahareh Moghtadaei[a,b,c], Loryn J. Bohne[b,c], Yingjie Liu[b,c], Pooja Krishnaswamy[a], Emmanuel E. Egom[a], Darrell D. Belke[b,c], Sara A. Rafferty[a], Martin Ezeani[a], Anne M. Gillis[b,c], and Robert A. Rose[a,b,c,2]

[a]Department of Physiology and Biophysics, Faculty of Medicine, Dalhousie University, Halifax, NS, Canada, B3H 4R2; [b]Libin Cardiovascular Institute of Alberta, Department of Cardiac Sciences, Cumming School of Medicine, University of Calgary, Calgary, AB, Canada, T2N 4Z6; and [c]Libin Cardiovascular Institute of Alberta, Department of Physiology and Pharmacology, Cumming School of Medicine, University of Calgary, Calgary, AB, Canada, T2N 4Z6

Edited by Christine E. Seidman, Howard Hughes Medical Institute, Brigham and Women's Hospital and Harvard Medical School, Boston, MA, and approved February 20, 2020 (received for review August 29, 2019)

Atrial fibrillation (AF) is prevalent in diabetes mellitus (DM); however, the basis for this is unknown. This study investigated AF susceptibility and atrial electrophysiology in type 1 diabetic Akita mice using in vivo intracardiac electrophysiology, high-resolution optical mapping in atrial preparations, and patch clamping in isolated atrial myocytes. qPCR and western blotting were used to assess ion channel expression. Akita mice were highly susceptible to AF in association with increased P-wave duration and slowed atrial conduction velocity. In a second model of type 1 DM, mice treated with streptozotocin (STZ) showed a similar increase in susceptibility to AF. Chronic insulin treatment reduced susceptibility and duration of AF and shortened P-wave duration in Akita mice. Atrial action potential (AP) morphology was altered in Akita mice due to a reduction in upstroke velocity and increases in AP duration. In Akita mice, atrial Na^+ current (I_{Na}) and repolarizing K^+ current (I_K) carried by voltage gated K^+ ($K_v1.5$) channels were reduced. The reduction in I_{Na} occurred in association with reduced expression of *SCN5a* and voltage gated Na^+ ($Na_V1.5$) channels as well as a shift in I_{Na} activation kinetics. Insulin potently and selectively increased I_{Na} in Akita mice without affecting I_K. Chronic insulin treatment increased I_{Na} in association with increased expression of $Na_V1.5$. Acute insulin also increased I_{Na}, although to a smaller extent, due to enhanced insulin signaling via phosphatidylinositol 3,4,5-triphosphate (PIP_3). Our study reveals a critical, selective role for insulin in regulating atrial I_{Na}, which impacts susceptibility to AF in type 1 DM.

atrial fibrillation | diabetes mellitus | phosphoinositide 3-kinase | action potential | Na^+ current

Atrial fibrillation (AF), the most common sustained arrhythmia encountered clinically (1, 2), is highly prevalent in diabetes mellitus (DM) (3–6). AF increases the risk of stroke and death and has a substantial negative impact on quality of life. While AF and DM share some common risk factors, it is also clear that DM is an independent risk factor for the development of AF (7, 8). Consistent with this, a longer duration of untreated DM or poor glycemic control independently and significantly increases the risk of developing AF (5, 9). Furthermore, AF is clearly associated with a worse prognosis in diabetic patients, greatly increasing the risk of adverse cardiovascular events and all-cause mortality (3, 6). Despite these links, the mechanisms leading to a substrate for AF in DM are not understood, which likely contributes to the limited efficacy of current AF therapies.

Type 1 DM, which affects up to 10% of the global diabetic population (10), is characterized by a lack of insulin production due to the loss of pancreatic β cells that results in hypoinsulinemia and hyperglycemia. Under normal conditions, insulin binds to its receptor and activates the phosphoinositide 3-kinase (PI3K) pathway (11, 12). Specifically, insulin activates PI3Kα, which phosphorylates phosphatidylinositol 4,5-bisphosphate (PIP_2) to produce the second messenger phosphatidylinositol 3,4,5-triphosphate (PIP_3). PIP_3 mediates many key effects of insulin, including in the heart (13, 14).

Electrical remodeling in the atria is known to be an important contributor to the creation of a substrate for AF (15, 16). At the cellular level, atrial action potential (AP) morphology is a major determinant of atrial electrophysiology. The upstroke velocity of the AP is determined by the Na^+ current (I_{Na}), which is a major contributor to atrial conduction velocity (17, 18). Cardiac I_{Na} is primarily carried by voltage gated Na^+ channels ($Na_V1.5$), which are encoded by the *SCN5a* gene. Alterations in atrial I_{Na} and AP upstroke velocity can affect atrial conduction velocity and the likelihood of electrical reentry, thereby affecting susceptibility to AF (2, 15). Action potential duration (APD) and repolarization of the AP are affected by the balance between several inward and outward currents, including the L-type Ca^{2+} current ($I_{Ca,L}$) and the late Na^+ current ($I_{Na,L}$), and the activity of a number of voltage gated K^+ (K_v) channels, including, among others, the transient outward K^+ current (I_{to}; carried by $K_V4.2/4.3$ channels)

Significance

Atrial fibrillation (AF) is prevalent in diabetic patients, yet the basis for AF in diabetes is poorly understood. We have used type 1 diabetic Akita mice to study the effects of insulin on atrial electrophysiology in diabetes. We demonstrate that Akita mice are highly susceptible to AF due to impaired electrical conduction and that insulin treatment can reduce the occurrence of this arrhythmia. Atrial action potential morphology was altered in Akita mice in association with reductions in atrial Na^+ current (I_{Na}) and repolarizing potassium current. Insulin treatment potently increased atrial I_{Na} via distinct chronic and acute effects. These experiments identify antiarrhythmic effects of insulin in type 1 diabetes via potent effects on atrial I_{Na}.

Author contributions: I.P., H.J.J., and R.A.R. designed research; I.P., H.J.J., T.L., M.M., L.J.B., Y.L., P.K., E.E.E., D.D.B., S.A.R., M.E., and R.A.R. performed research; I.P., H.J.J., T.L., M.M., L.J.B., Y.L., D.D.B., A.M.G., and R.A.R. analyzed data; and I.P., H.J.J., A.M.G., and R.A.R. wrote the paper.

The authors declare no competing interest.

This article is a PNAS Direct Submission.

[1]I.P and H.J.J. contributed equally to this work.

[2]To whom correspondence may be addressed. Email: robert.rose@ucalgary.ca.

This article contains supporting information online at https://www.pnas.org/lookup/suppl/doi:10.1073/pnas.1914853117/-/DCSupplemental.

First published March 20, 2020.

and the ultrarapid delayed rectifier K^+ current (I_{Kur}; an atrial-specific current carried by $K_V1.5$ channels).

The goal of the present study was to investigate atrial electrophysiology and the basis for AF in type 1 DM. Our studies were conducted using the Akita mouse model of type 1 DM as well as wild-type mice injected with streptozotocin (STZ) (19, 20). Each of these is a well-validated model of type 1 DM (19). Our data demonstrate that Akita and STZ-injected mice are highly susceptible to induced AF. Furthermore, AF inducibility is reduced by insulin treatment in Akita mice. Our mechanistic studies show that AF in Akita mice is associated with alterations in atrial AP morphology and that insulin has distinct acute and chronic effects on AP morphology and I_{Na} in the atria.

Results

Susceptibility to AF in Type 1 Diabetic Mice. Burst pacing was used to assess susceptibility to AF (Fig. 1*A*) in anesthetized wild-type and Akita mice. Blood glucose was elevated in Akita mice compared with wild types (*SI Appendix*, Fig. S1*A*). Strikingly, Akita mice were highly susceptible to induced AF compared with wild-type mice (Fig. 1*B*). The episodes of AF induced in two wild-type mice were very brief, lasting less than 5 s (Fig. 1*C*). In contrast, AF induced in Akita mice was longer in duration. Specifically, 62% of the Akita mice had AF between 5 and 30 s, and 23% of Akita mice were induced into AF lasting longer than 30 s (Fig. 1*C* and *SI Appendix*, Table S1). To ensure that these observations were not specific to the Akita model of type 1 DM, we also investigated AF susceptibility in a second model of type 1 DM secondary to STZ injection in wild-type mice. STZ injection led to hyperglycemia as indicated by increases in blood glucose (*SI Appendix*, Fig. S2*A*). Furthermore, STZ-injected mice displayed similar increases in AF inducibility (*SI Appendix*, Fig. S2 *B* and *C*) and AF duration (*SI Appendix*, Fig. S2*D* and Table S2) to Akita mice. Together, these data illustrate that both mouse models of type 1 DM display increased susceptibility to AF.

Next, we assessed the effects of chronic insulin treatment on AF burden in Akita mice. Insulin pellet implantation reduced blood glucose levels in Akita mice to levels that were similar to wild types, while placebo pellets had no effect on blood glucose in Akita mice (*SI Appendix*, Fig. S1*B*). Following chronic insulin treatment, only 25% of Akita mice were induced into AF compared with 62% of placebo-treated Akita mice (Fig. 1*D*). In addition, when AF was induced in insulin-treated Akita mice, the episodes were brief, lasting less than 5 s in 83% of the mice. No insulin-treated Akita mice had AF lasting longer than 30 s (Fig. 1*E* and *SI Appendix*, Table S3). In contrast, 50% of placebo-treated Akita mice demonstrated AF lasting longer than 5 s, and in some cases, it lasted longer than 30 s (Fig. 1*E* and *SI Appendix*, Table S3). These data demonstrate that chronic insulin treatment reduced both the susceptibility and the duration of AF in Akita mice.

We also examined the effects of acute insulin treatment on AF in Akita mice. Acute intraperitoneal injection of insulin (5 to 10 U/kg) reduced blood glucose in Akita mice to values similar to wild-type mice within 30 to 45 min, while saline-injected Akita mice were unaffected (*SI Appendix*, Fig. S1*C*). Acute insulin injection had no effect on inducibility of AF in Akita mice (Fig. 1*F* and *SI Appendix*, Table S4); however, the median AF duration was lower in Akita mice following acute insulin treatment (Fig. 1*G*).

Atrial Electrophysiology in Type 1 Diabetic Mice. P-wave duration and P wave–R wave (PR) intervals were assessed in Akita mice and STZ-treated mice. Compared with wild types, Akita mice had prolonged P-wave duration (Fig. 2*A*–*C*) and PR intervals (*SI Appendix*, Table S5). P-wave duration and PR interval were also

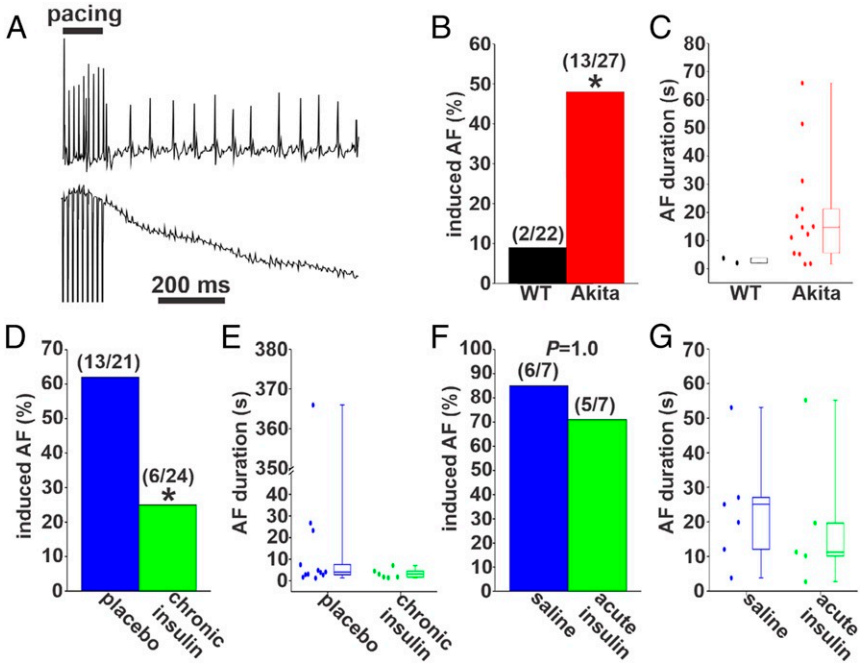

Fig. 1. AF in untreated Akita mice and Akita mice treated with insulin. (*A*) Representative surface (*Upper*) and intracardiac atrial (*Lower*) ECGs showing the induction of AF in an untreated anesthetized Akita mouse following burst pacing. (*B*) Inducibility of AF in untreated wild-type (WT) and Akita mice. Numbers in parentheses indicate the number of mice induced into AF following burst pacing. $^*P < 0.05$ by Fisher's exact test. (*C*) Duration of AF in the WT ($n = 2$) and Akita ($n = 13$) mice that were induced into AF. (*D*) Inducibility of AF in Akita mice treated chronically with insulin or placebo for 4 wk. $^*P < 0.05$ vs. placebo by Fisher's exact test. (*E*) Duration of AF in the placebo- ($n = 13$) and insulin-treated ($n = 6$) Akita mice that were induced into AF. (*F*) Inducibility of AF in Akita mice treated acutely with insulin or saline. Data were analyzed by Fisher's exact test. (*G*) Summary data demonstrating the duration of AF in the saline- ($n = 7$) and insulin-treated ($n = 5$) Akita mice that were induced into AF. *SI Appendix*, Tables S1–S4 have additional AF analysis.

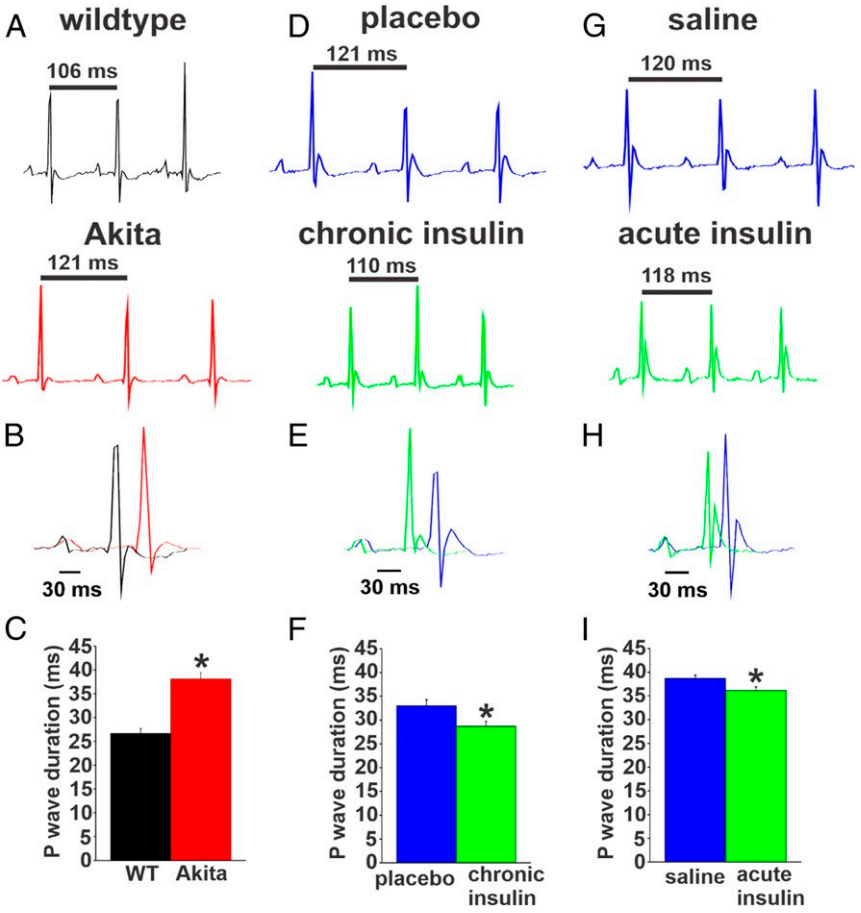

Fig. 2. P-wave duration in untreated Akita mice and Akita mice treated with insulin. (*A*) Representative surface ECGs from untreated wild-type (WT) and Akita mice. (*B*) Overlay of ECGs from WT and Akita mice. (*C*) Summary of P-wave duration in untreated WT and Akita mice. $n = 7$ WT mice and 10 Akita mice. $^*P < 0.05$ vs. WT by Student's *t* test. (*D*) Representative surface ECGs from Akita mice treated chronically with insulin or placebo pellets for 4 wk. (*E*) Overlay of ECGs from Akita mice treated chronically with insulin or placebo pellets. (*F*) Summary of the effects of chronic insulin on P-wave duration in Akita mice. $n = 21$ placebo-treated mice and 22 insulin-treated mice. $^*P < 0.05$ vs. placebo by Student's *t* test. (*G*) Representative surface ECGs from Akita mice treated acutely with insulin or saline by intraperitoneal injection. (*H*) Overlay of ECGs from Akita mice treated acutely with insulin. (*I*) Summary of the effects of acute insulin treatment on P-wave duration in Akita mice. $n = 8$ saline-treated mice and 7 insulin-treated mice. *SI Appendix,* Tables S5–S8 has additional ECG analysis. $^*P < 0.05$ vs. placebo by Student's *t* test.

prolonged in STZ-treated mice (*SI Appendix*, Fig. S2 *E* and *F* and Table S6). Chronic insulin treatment shortened P-wave duration (Fig. 2 *D–F*) and tended to reduce the PR interval in Akita mice compared with placebo controls (*SI Appendix*, Table S7). Acute insulin treatment also shortened P-wave duration in Akita mice (Fig. 2 *G–I*), although this effect was smaller in magnitude compared with chronic insulin treatment. These findings indicate that atrial conduction is impaired in type 1 diabetic mice and improved following chronic as well as acute insulin treatment.

Patterns of atrial conduction in Akita mice were assessed using high-resolution optical mapping in isolated atrial preparations from wild-type and Akita mice. Representative activation maps (Fig. 3*A*) illustrate that conduction initiates in the right atrial posterior wall and then spreads across the full atrial preparation (21–23). These representative maps show that total conduction time across the full atrial preparation is longer in Akita mice. We also quantified local conduction velocities within the right and left atrial appendage regions. Right and left atrial conduction velocities were both reduced in Akita mice compared with the wild types (Fig. 3*B*), further confirming that atrial conduction is impaired in Akita mice. Consistent with the changes in P-wave duration measured in vivo, optical mapping studies also demonstrate that chronic insulin treatment in Akita mice resulted in faster conduction time across the atria (Fig. 3*C*) and increased right and left atrial conduction velocities (Fig. 3*D*).

Echocardiographic assessment (*SI Appendix*, Fig. S3 and Table S9) demonstrates that Akita mice did not display substantial changes in ventricular structure or function, which is consistent with prior studies (24). Although maximum left atrial area was modestly increased in Akita mice, other measures of atrial size were similar between wild-type and Akita mice (*SI Appendix*, Fig. S3 and Table S9). Serum $[Na^+]$ and $[Cl^-]$ were modestly reduced, while serum $[K^+]$ and $[Ca^{2+}]$ were not altered in Akita mice compared with wild-type controls (*SI Appendix*, Fig. S4).

Alterations in Atrial Myocyte Electrophysiology in Akita Mice. To further investigate the basis for increased AF and impaired atrial conduction in Akita mice, we measured APs in isolated right and left atrial myocytes (Fig. 4 *A* and *B*). Consistent with the absence of major changes in atrial size, there were no differences in cell capacitance in right atrial myocytes (50.6 ± 5.1 vs. 52.9 ± 7.3 pF; $P = 0.84$) or left atrial myocytes (54 ± 4.1 vs. 58.8 ± 5.8 pF; $P = 0.50$) between wild-type and Akita mice, indicating no differences in cell size. AP upstroke velocity (maximum upstroke velocity [V_{max}]) was reduced in right and left atrial myocytes from Akita mice compared with wild-type controls (Fig. 4 *C* and *D*). Furthermore, APD was prolonged throughout repolarization

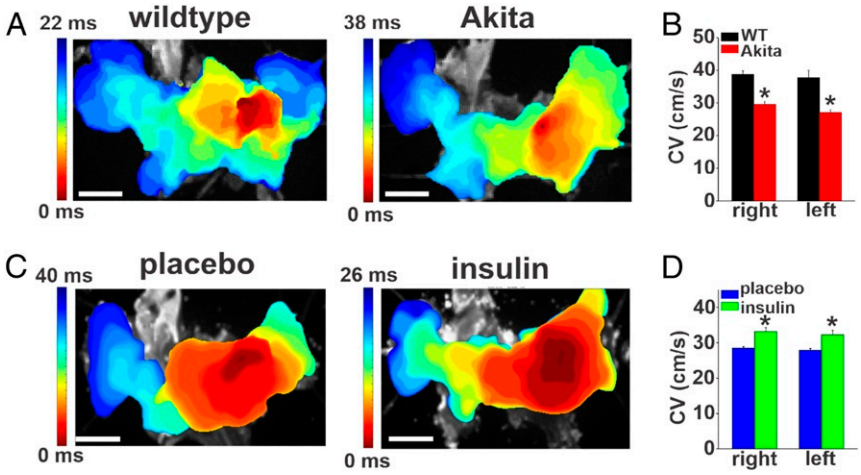

Fig. 3. Patterns of electrical conduction in the atria in untreated Akita mice and Akita mice treated chronically with insulin. (*A*) Representative activation maps in isolated atrial preparations from wild-type (WT) and untreated Akita mice. The right atrial appendage is on the right side of the image. Red indicates the earliest activation time. The color scale indicates total conduction time across the atrial preparation. (Scale bar: 3 mm.) (*B*) Summary of local right and left atrial conduction velocities (CV) (*SI Appendix, Supplemental Methods*) in WT and Akita mice. $n = 7$ WT and 8 Akita hearts. $^*P < 0.05$ vs. WT by two-way ANOVA with Tukey's post hoc test. (*C*) Representative activation maps in atrial preparations from Akita mice treated with placebo or chronically with insulin for 4 wk. (*D*) Summary of local right and left atrial conduction velocities in placebo- and insulin-treated Akita mice. $n = 6$ placebo- and 5 insulin-treated Akita hearts. $^*P < 0.05$ vs. placebo by two-way ANOVA with Tukey's post hoc test.

in both right and left atrial myocytes from Akita mice (Fig. 4 *E* and *F*). These alterations in AP morphology occurred without changes in resting membrane potential (*SI Appendix*, Tables S10 and S11).

To ensure that the changes in APD observed in isolated cells were not a consequence of cell isolation procedures, we also measured APDs in wild-type and Akita mice using optical mapping (*SI Appendix*, Fig. S5). Optical APs measured in the right and left atria of intact atrial preparations confirm that APD was prolonged in Akita mice (*SI Appendix*, Fig. S5).

AP morphology was also assessed in isolated ventricular myocytes from wild-type and Akita mice (*SI Appendix*, Fig. S6 and Table S12). APD was prolonged in Akita ventricular myocytes; however, in contrast to atrial myocytes, there were no differences in AP V_{max} in Akita ventricular myocytes.

The alterations in atrial conduction (prolonged P-wave duration, reduced atrial conduction velocity) as well as the reduction in atrial AP V_{max} in Akita mice are suggestive of changes in atrial I_{Na}. Accordingly, we measured I_{Na} in isolated right and left atrial myocytes from wild-type and Akita mice (Fig. 5*A* and *SI Appendix*, Fig. S7). Summary current–voltage (IV) curves for right atrial myocytes demonstrate that I_{Na} is reduced in Akita mice (Fig. 5*B*). I_{Na} activation curves (Fig. 5*C*) and analysis of I_{Na} activation kinetics (*SI Appendix*, Table S13) demonstrate that the reduction in I_{Na} density in Akita mice occurred in association with a reduction in maximum conductance (G_{max}) and a modest (~3-mV) rightward shift in the voltage dependence of activation [$V_{1/2(act)}$]. Similar alterations in I_{Na} density, G_{max}, and activation kinetics were observed in left atrial myocytes from Akita mice (*SI Appendix*, Fig. S7 and Table S13). We also measured steady-state inactivation in right atrial myocytes in Akita mice (*SI Appendix*, Fig. S8). Voltage dependence of inactivation was not altered in Akita right atrial myocytes.

Because the reductions in I_{Na} density and G_{max} were large relative to the shift in $V_{1/2(act)}$, we also measured the expression of *SCN5a* messenger ribonucleic acid (mRNA) as well as $Na_V1.5$ protein in the atria of wild-type and Akita mice. These data show that expressions of *SCN5a* (Fig. 5*D* and *SI Appendix*, Fig. S7*D*) and $Na_V1.5$ (Fig. 5*E* and *SI Appendix*, Fig. S7*E*) were reduced in the right and left atria of Akita mice compared with wild-type controls.

Next, we investigated the properties and expression of repolarizing K^+ current (I_K) in order to assess the ionic basis for the prolongation in atrial APD observed in Akita mice. We first measured I_K in right atrial myocytes from wild-type and Akita mice. I_K was measured with and without a prepulse to inactivate I_{to} (25, 26) (Fig. 6*A* and *SI Appendix*, *Supplemental Methods*). Summary I_K IV relationships illustrate that peak total (i.e., no prepulse) I_K was reduced in Akita mice at membrane potentials positive to +20 mV (Fig. 6*B*). Consistent with the lack of differences in resting membrane potential, there were no differences in I_K in the region of the IV curves where inward rectifier K^+ current (I_{K1}) is active (i.e., negative to −80 mV) between wild-type and Akita mice. IV curves for peak I_K measured from the protocols with an inactivating prepulse demonstrate that I_K remained reduced in Akita mice at membrane potentials positive to +20 mV (Fig. 6*C*) when I_{to} is inactivated. In agreement with these observations, IV relationships for I_{to} (i.e., the difference current between measurements with and without the inactivating prepulse) illustrate no differences between wild-type and Akita mice (Fig. 6*D*). Very similar observations were made for I_K in left atrial myocytes from wild-type and Akita mice (*SI Appendix*, Fig. S9). Further evidence that the reduction in repolarizing I_K in Akita mice does not involve I_{to} was obtained from western blot studies, which show no differences in the protein levels of $K_V4.2$ and $K_V4.3$ in right and left atria from wild-type and Akita mice (*SI Appendix*, Fig. S10).

The I_{Kur} carried by $K_V1.5$ channels was investigated by measuring the component of I_K sensitive to 4-aminopyridine (4-AP) (100 μM) (Fig. 6*E*) (26, 27) in right atrial myocytes from wild-type and Akita mice. From these representative recordings, it is apparent that outward I_K is smaller at baseline and that the reduction in I_K elicited by 4-AP was smaller in Akita mice. These recordings also demonstrate that the effects of 4-AP were reversible on washout. Summary data confirm that the 4-AP–sensitive current (i.e., $K_V1.5$-mediated I_{Kur}) is reduced in Akita mice (Fig. 6*F*). The expression of the *KCNA5* gene (which encodes $K_V1.5$) was not different in Akita mice (*SI Appendix*, Fig. S11*A*); however, in agreement with the reduction in current, $K_V1.5$ protein in Akita right atrium was reduced compared with wild-type controls (*SI Appendix*, Fig. S11*B*).

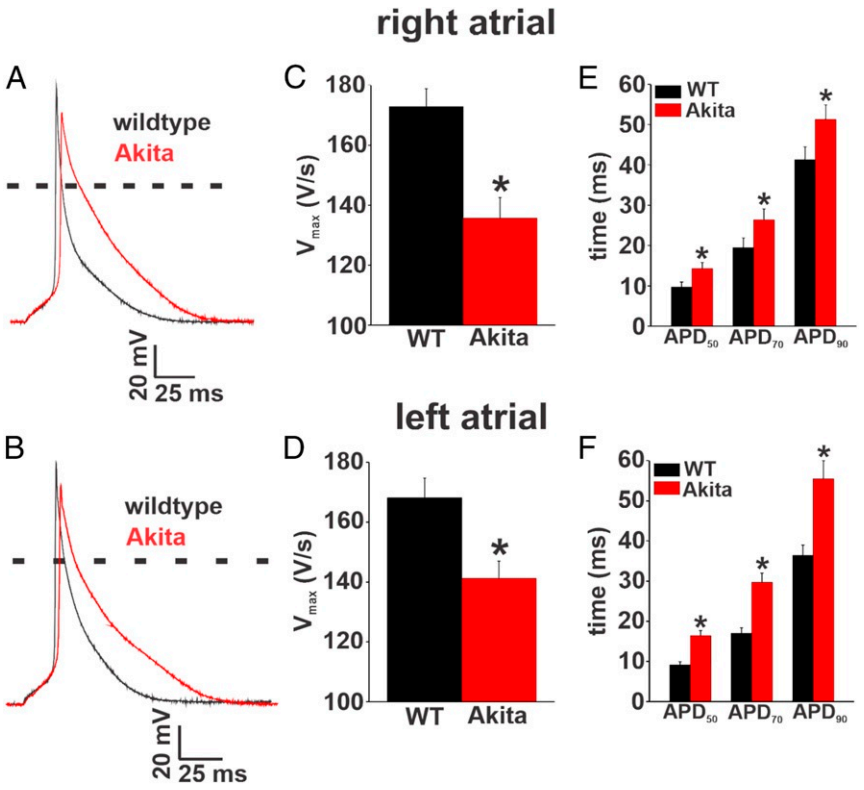

Fig. 4. Right and left atrial AP morphology in Akita mice. (*A* and *B*) Representative stimulated APs in isolated right atrial (*A*) and left atrial (*B*) myocytes from wild-type (WT) and Akita mice. (*C* and *D*) Summary of AP V_{max} in isolated right atrial (*C*) and left atrial (*D*) myocytes from WT and Akita mice. (*E* and *F*) Summary of APD in isolated right atrial (*E*) and left atrial (*F*) myocytes from WT and Akita mice. APD was measured at 50% (APD_{50}), 70% (APD_{70}), and 90% (APD_{90}) repolarization. For right atrial myocytes, $n = 18$ for the WT and 16 for Akita. For left atrial myocytes, $n = 12$ for the WT and 11 for Akita. *SI Appendix*, Tables S10 and S11 has additional AP analysis. $^*P < 0.05$ vs. the WT by Student's *t* test.

APD can also be affected by other currents, such as $I_{Ca,L}$ and $I_{Na,L}$, which were both assessed in Akita right atrial myocytes. $I_{Ca,L}$ (*SI Appendix*, Fig. S12) and $I_{Na,L}$ (*SI Appendix*, Fig. S13) were not different between wild-type and Akita mice. There were also no differences in atrial calcium transient morphology between wild-type and Akita mice (*SI Appendix*, Fig. S14). As

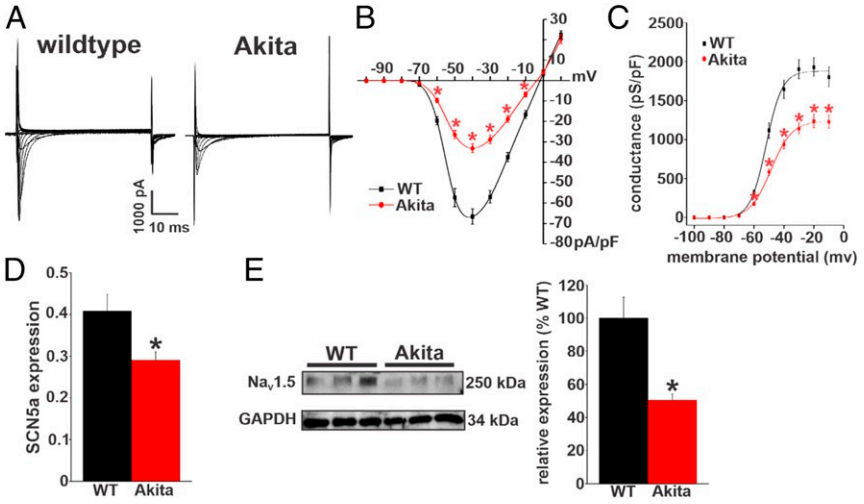

Fig. 5. I_{Na} is reduced in right atrial myocytes in Akita mice. (*A*) Representative I_{Na} recordings in right atrial myocytes isolated from wild-type (WT) and Akita mice. Cell capacitance for these representative recordings was 44 pF for the WT and 41 pF for Akita. (*B*) I_{Na} IV curves in right atrial myocytes isolated from WT and Akita mice. Current densities are measured in picoamperes/picofarad (pA/pF). (*C*) Summary I_{Na} activation curves in right atrial myocytes from WT and Akita mice. Conductance is measured in picosiemens/picofarad (pS/pF); $n = 21$ myocytes for the WT and 18 for Akita. I_{Na} activation kinetics are summarized in *SI Appendix*, Table S13. $^*P < 0.05$ vs. the WT at each membrane potential by two-way repeated measures ANOVA with Tukey's post hoc test. (*D*) *SCN5a* mRNA expression in the right atrium in WT and Akita mice. $n = 23$ WT and 15 Akita mice. $^*P < 0.05$ vs. the WT by Student's *t* test. (*E*) $Na_V1.5$ protein expression in the right atrium in WT and Akita mice. $n = 6$ WT and 6 Akita mice. $^*P < 0.05$ vs. the WT by Student's *t* test.

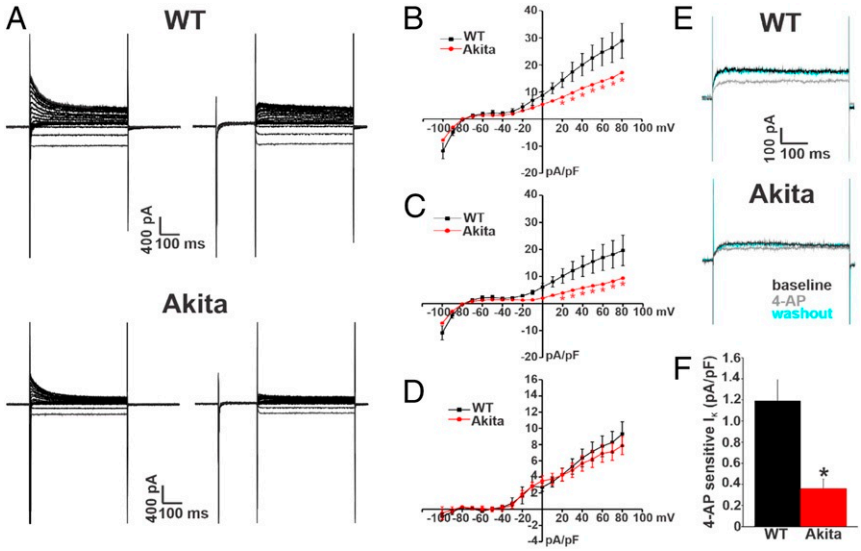

Fig. 6. Repolarizing I_K is reduced in right atrial myocytes in Akita mice. (*A*) Representative I_K recordings in right atrial myocytes isolated from wild-type (WT) and Akita mice. The recordings on the left represent total I_K measured between −100 and +80 mV. The recordings on the right represent I_K measured between −100 and +80 mV following a prepulse to −40 mV to inactivate I_{to}. Cell capacitances for these representative recordings were 33 pF for the WT and 38 pF for Akita. (*B*) Summary I_K IV curves measured at the peak of the I_K recordings without the prepulse (recordings on the left in *A*) for right atrial myocytes isolated from WT and Akita mice. (*C*) Summary I_K IV curves measured at the peak of the I_K recordings with the prepulse (recordings on the right in *A*) for right atrial myocytes isolated from WT and Akita mice. $^*P < 0.05$ vs. the WT at each membrane potential by two-way repeated measures ANOVA with Tukey's post hoc test. (*D*) Summary I_K IV curves for the difference current between *B* and *C*, which is a measure of I_{to}. $P = 0.85$ for I_{to} density between the WT and Akita by two-way repeated measures ANOVA. For *B*–*D*, $n = 19$ WT and 16 Akita right atrial myocytes. (*E*) Representative I_K recordings at +30 mV illustrating the effects of 4-AP (100 μM), which inhibits $K_V1.5$-mediated I_K, in right atrial myocytes from WT and Akita mice. (*F*) Summary data illustrating the amplitude of the 4-AP–sensitive I_K in right atrial myocytes from WT and Akita mice. $n = 9$ WT and 10 Akita right atrial myocytes. $^*P < 0.05$ vs. the WT by Student's *t* test. Current densities are measured in picoamperes/picofarad (pA/pF).

atrial electrical function is also affected by connexins, we measured the expression of *GJA5* and *GJA1* mRNAs, which encode Cx40 and Cx43, in the right atrium. *GJA5* and *GJA1* expressions were not altered in Akita mice (*SI Appendix*, Fig. S15).

Increases in APD could lead to the occurrence of triggered activity in the form of early afterdepolarizations (EADs). To assess this possibility, APs were measured at different pacing frequencies at baseline and in the presence of isoproterenol (1 μM). No EADs were observed in wild-type or Akita right atrial myocytes in these studies (*SI Appendix*, Fig. S16).

Effects of Chronic and Acute Insulin Treatment on Atrial Myocyte Electrophysiology in Akita Mice. To investigate the basis for the beneficial effects of insulin on AF susceptibility and atrial conduction, we next examined the effects of chronic insulin treatment on atrial myocyte AP morphology (Fig. 7*A*). AP V_{max} was substantially increased following insulin treatment in Akita mice (Fig. 7*B*). In contrast, insulin treatment had no effect on action potential duration measured at 50% repolarization (APD_{50}), action potential duration measured at 70% repolarization (APD_{70}), or action potential duration measured at 90% repolarization (APD_{90}) compared with placebo controls (Fig. 7*C* and *SI Appendix*, Table S14) so that APD remained prolonged in treated Akita mice (compare with wild-type values in Fig. 4).

Next, we measured right atrial I_{Na} in Akita mice treated chronically with insulin or placebo (Fig. 7*D*). Summary IV curves demonstrate that atrial I_{Na} was increased in Akita mice following chronic insulin treatment (Fig. 7*E*). Furthermore, I_{Na} activation curves (Fig. 7*F*) and kinetic analysis (*SI Appendix*, Table S13) demonstrate that chronic insulin increased I_{Na} in association with an increase in G_{max}, but there were no differences in $V_{1/2(act)}$ or slope factor. Western blot studies (Fig. 7*G*) illustrate that chronic insulin treatment increased the levels of $Na_V1.5$ in the atria in Akita mice.

Consistent with the lack of effect of insulin on atrial APD, insulin treatment had no effect on I_K (with or without an inactivating prepulse) in Akita mice (*SI Appendix*, Fig. S17). Furthermore, chronic insulin treatment did not affect $K_V1.5$ protein levels in Akita mice compared with placebo-treated controls (*SI Appendix*, Fig. S18).

We next sought to assess the effects of enhancing insulin signaling acutely (i.e., intraperitoneal injection of insulin) in Akita mice. Immediately following the reduction in blood glucose from acute insulin injection, right atrial myocytes were isolated, and AP morphology was assessed (Fig. 8*A*). Summary data illustrate that AP V_{max} was increased by acute insulin injection in Akita mice (Fig. 8*B*) but that APD_{50}, APD_{70}, and APD_{90} were unaffected compared with saline controls (Fig. 8*C* and *SI Appendix*, Table S15). Notably, the increase in V_{max} was smaller after acute insulin compared with chronic insulin (*SI Appendix*, Fig. S19*A*).

Next, we measured I_{Na} in Akita right atrial myocytes isolated after acute insulin (or saline) injection (Fig. 8*D*). I_{Na} density was increased following acute insulin injection (Fig. 8*E*). This increase occurred in association with an increase in G_{max}, but there were no changes in $V_{1/2(act)}$ or slope factor (Fig. 8*F* and *SI Appendix*, Table S13) compared with saline controls. The increase in I_{Na} elicited by acute insulin was smaller than after chronic insulin (*SI Appendix*, Fig. S19*B*). Acute insulin injection had no effects on I_K in Akita atrial myocytes (*SI Appendix*, Fig. S20).

The role of acute insulin signaling was further investigated by dialyzing right atrial myocytes from Akita mice with PIP_3 [a direct mediator of insulin signaling downstream of the insulin receptor and PI3K (12, 14)] or PIP_2 (not a second messenger directly activated by insulin) as a control. Cells were dialyzed with these phospholipids (1 μM) for 10 min, and then, atrial AP morphology was assessed (Fig. 8*G*). Summary data illustrate that PIP_3 increased V_{max} (Fig. 8*H*) to a similar extent as acute insulin (*SI Appendix*, Fig. S19*A*) but had no effects on APD (Fig. 8*I* and

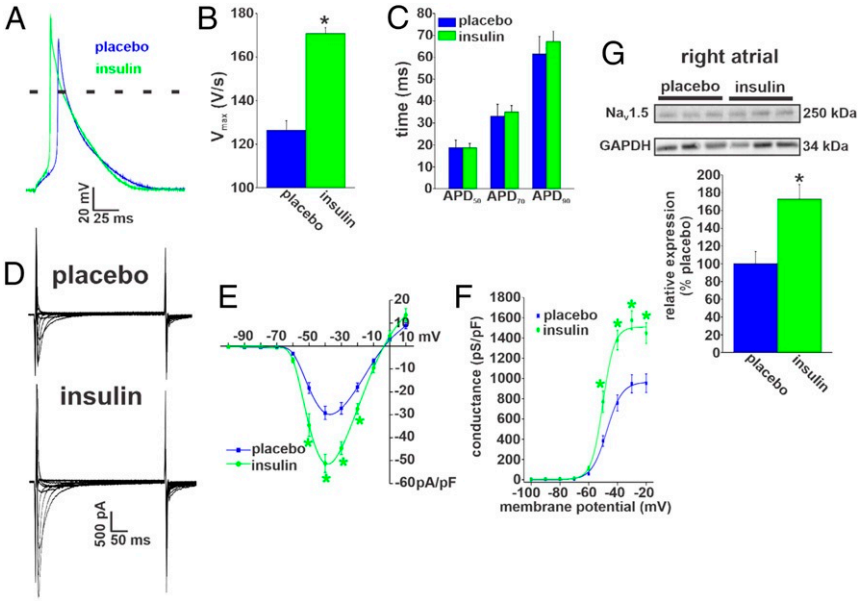

Fig. 7. Effects of chronic insulin treatment on atrial AP morphology and I_{Na} in Akita mice. (*A*) Representative right atrial APs in Akita mice treated with insulin or placebo for 4 wk. (*B*) Summary of the effects of chronic insulin on right atrial AP V_{max} in Akita mice. $^*P < 0.05$ vs. placebo by Student's *t* test. (*C*) Summary of the effects of chronic insulin on right atrial APD in Akita mice. Chronic insulin had no effect on APD compared with placebo. For AP measurements, $n = 19$ myocytes for placebo and 14 for chronic insulin treatment. *SI Appendix*, Table S14 has additional analysis of AP morphology. (*D*) Representative I_{Na} recordings in right atrial myocytes isolated from Akita mice treated chronically with insulin or placebo for 4 wk. Cell capacitances for these representative recordings were 31 pF for the wild type and 30 pF for Akita. (*E*) Summary I_{Na} IV curves for right atrial myocytes from Akita mice treated chronically with insulin or placebo. Current densities are measured in picoamperes/picofarad (pA/pF). (*F*) Summary I_{Na} activation curves for right atrial myocytes isolated from Akita mice treated chronically with insulin or placebo. $n = 18$ myocytes for placebo and 13 myocytes for chronic insulin treatment. *SI Appendix*, Table S13 has additional I_{Na} kinetic analysis. $^*P < 0.05$ vs. placebo by two-way repeated measures ANOVA with Tukey's post hoc test. Conductance is measured in picosiemens/picofarad (pS/pF). (*G*) $Na_V1.5$ protein expression in the right atrium of Akita mice treated chronically with insulin or placebo. $n = 6$ placebo-treated and 6 insulin-treated right atria. $^*P < 0.05$ vs. placebo by Student's *t* test.

SI Appendix, Table S16) compared with PIP_2-treated myocytes. Akita myocytes dialyzed with PIP_2 were very similar to untreated Akita atrial myocytes (compare with Fig. 4).

Consistent with its effects on V_{max}, PIP_3 also increased atrial I_{Na} density in comparison with cells dialyzed with PIP_2 (Fig. 8 *J* and *K*). This increase in I_{Na} was also similar to that seen following acute insulin treatment (*SI Appendix*, Fig. S19*B*). In addition, PIP_3 increased I_{Na} G_{max} without affecting $V_{1/2(act)}$ or slope factor in Akita atrial myocytes (Fig. 8*L* and *SI Appendix*, Table S13). PIP_3 had no effect on I_K in Akita atrial myocytes (*SI Appendix*, Fig. S21). Collectively, these data demonstrate that acutely enhancing insulin signaling selectively increases AP V_{max} and I_{Na} density in Akita atrial myocytes via PIP_3 signaling without affecting APD or repolarizing I_K.

Protein Kinase C Inhibition Increases I_{Na} in Akita Atrial Myocytes. The data above demonstrate that enhancing insulin signaling increased atrial I_{Na} in Akita mice. These effects of insulin occurred without changes in $V_{1/2(act)}$; however, our data also demonstrate that the reduction in I_{Na} in Akita mice is associated with a modest but significant shift in $V_{1/2(act)}$ (*SI Appendix*, Table S13). It has been shown that protein kinase C (PKC) is elevated in the hearts of Akita mice (28), and PKC is a well-known modulator of the biophysical properties of I_{Na} (29). Accordingly, we tested the hypothesis that elevated PKC contributes to the reduction in atrial I_{Na} by dialyzing right atrial myocytes from Akita mice with the PKC inhibitor bisindolylmaleimide 1 (30) (BIM1; 1 μM) (*SI Appendix*, Fig. S22). Compared with untreated Akita atrial myocytes, BIM1 increased I_{Na} density in Akita atrial myocytes (*SI Appendix*, Fig. S22*B*). Furthermore, I_{Na} activation curves (*SI Appendix*, Fig. S22*C*) and kinetic analysis (*SI Appendix*, Table S13) illustrate that BIM1 application increased I_{Na} G_{max} and elicited a left shift in the $V_{1/2(act)}$. BIM1 also tended to reduce the slope factor on the activation curve (*SI Appendix*, Table S13). These findings indicate that enhanced PKC activity in the atria of Akita mice contributes to the reduction in I_{Na} in association with a shift in I_{Na} activation kinetics.

Discussion

The present study demonstrates that, consistent with the human diabetic population (3, 5, 7), Akita and STZ-injected mice are highly susceptible to induced AF and that, when it occurred, AF was longer lasting in type 1 diabetic mice compared with wild-type controls. The increase in AF burden was associated with a prolongation of P-wave duration in Akita and STZ-injected mice, indicating that AF in type 1 DM is associated with impaired atrial electrical conduction. Akita and STZ-injected mice are well-established models of nonobese type 1 DM that are known to recapitulate many of the complications that occur in human DM (19, 31). Our observation that Akita and STZ mice also display increased susceptibility to AF establishes that these mice are excellent models of human type 1 DM that can be used for studying the relationships between DM and AF.

In further support of atrial electrical remodeling, we found that atrial AP morphology was substantially altered in Akita mice due to a reduction in V_{max} and increases in APD in association with reductions in atrial I_{Na} and I_{Kur}. While APD was also prolonged in ventricular myocytes in Akita mice, ventricular V_{max} was not significantly altered, suggesting that the reduction in V_{max} (and hence, the underlying I_{Na}) in Akita mice may be restricted to the atria. On the other hand, a previous study did report a reduction in ventricular I_{Na} in type 1 diabetic rabbits (alloxan induced) (32). A prior study also demonstrated that ventricular APD is prolonged in Akita mice due, at least in part, to an increase in $I_{Na,L}$ (33), whereas we did not observe any changes in $I_{Na,L}$ in Akita atrial myocytes. Prior studies have also

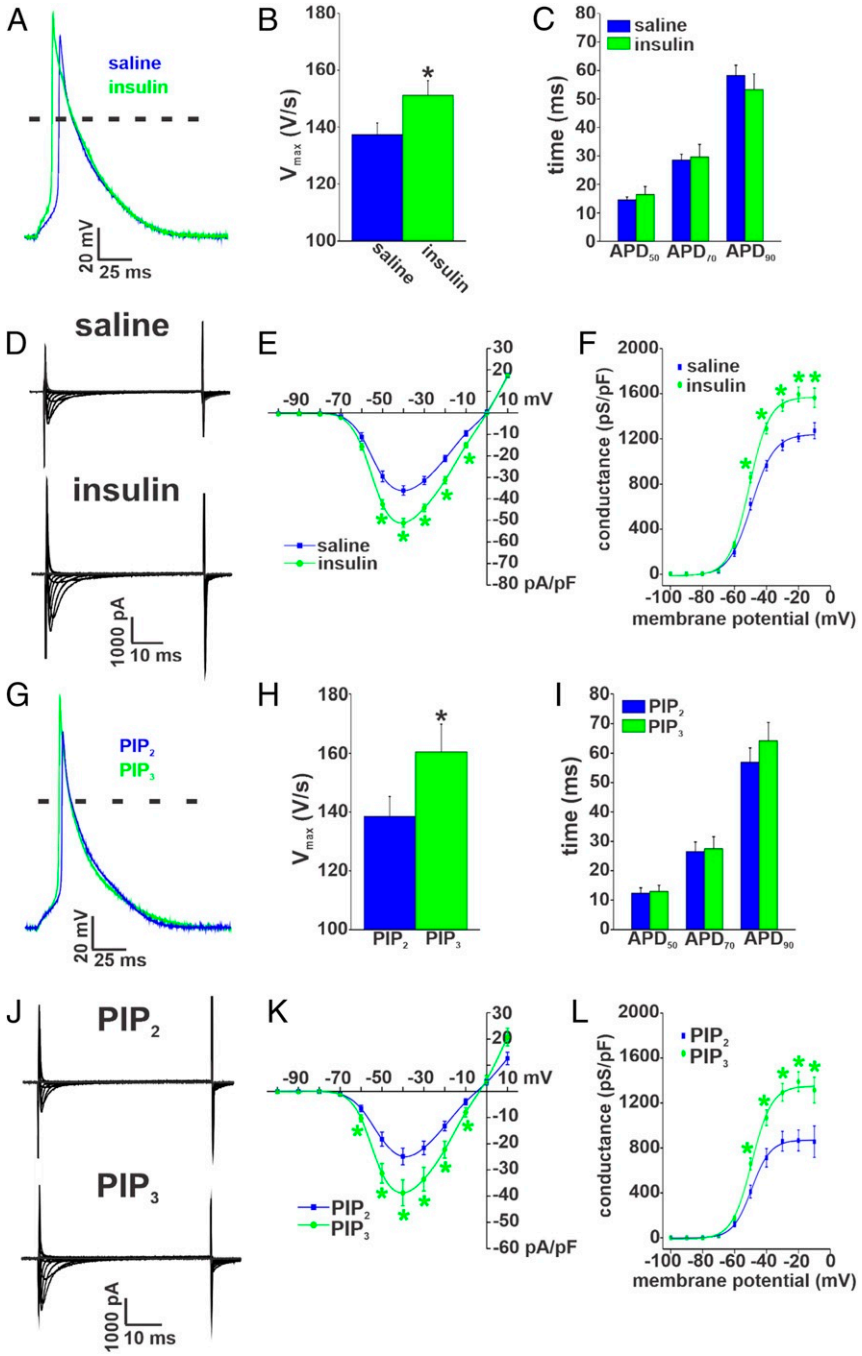

Fig. 8. Effects of acute insulin treatment and PIP_3 on atrial AP morphology and I_{Na} in Akita mice. (*A*) Representative right atrial APs in Akita mice treated acutely with insulin or saline. (*B*) Summary of the effects of acute insulin on right atrial AP V_{max} in Akita mice. $^*P < 0.05$ vs. saline by Student's *t* test. (*C*) Summary of the effects of acute insulin on right atrial APD in Akita mice. Acute insulin had no effect on right atrial APD compared with saline. For AP measurements, $n = 14$ myocytes for saline and 18 myocytes for acute insulin treatment. *SI Appendix*, Table S15 has additional analysis of AP morphology. (*D*) Representative I_{Na} recordings in right atrial myocytes isolated from Akita mice treated acutely with insulin or saline. Cell capacitances for these representative recordings were 42 pF for the wild type and 45 pF for Akita. (*E*) Summary I_{Na} IV curves for right atrial myocytes from Akita mice treated acutely with insulin or saline. Current densities are measured in picoamperes/picofarad (pA/pF). (*F*) Summary I_{Na} activation curves for right atrial myocytes isolated from Akita mice treated acutely with insulin or saline. $n = 8$ myocytes for saline and 12 myocytes for acute insulin treatment. *SI Appendix*, Table S13 has additional analysis of I_{Na} activation kinetics. $^*P < 0.05$ vs. saline at each membrane potential by two-way repeated measures ANOVA with Tukey's post hoc test. Conductance is measured in picosiemens/picofarad (pS/pF). (*G*) Representative APs in right atrial myocytes from Akita mice following dialysis with PIP_3 (1 μM) or PIP_2 (1 μM) as a control. Data are from cells dialyzed with phospholipids for 10 min. (*H*) Summary of the effects of PIP_3 on right atrial AP V_{max} in Akita mice. $^*P < 0.05$ vs. PIP_2 by Student's *t* test. (*I*) Summary of the effects of PIP_3 on right atrial APD in Akita mice. PIP_3 had no effect on right atrial APD. For AP measurements, $n = 7$ myocytes for PIP_2 and 8 myocytes for PIP_3. *SI Appendix*, Table S16 has additional analysis of AP morphology. (*J*) Representative I_{Na} recordings in right atrial myocytes from Akita mice following dialysis with PIP_3 (1 μM) or PIP_2 (1 μM) for 10 min. Cell capacitances for these representative recordings were 39 pF for the wild type and 38 pF for Akita. (*K*) Summary I_{Na} IV curves for right atrial myocytes from Akita mice following dialysis with PIP_3 or PIP_2. (*L*) Summary I_{Na} activation curves for right atrial myocytes from Akita mice following dialysis with PIP_3 or PIP_2. $n = 10$ myocytes for PIP_2 and 17 myocytes for PIP_3. *SI Appendix*, Table S13 has additional analysis of I_{Na} activation kinetics. $^*P < 0.05$ vs. PIP_2 by two-way repeated measures ANOVA with Tukey's post hoc test.

demonstrated that $I_{Ca,L}$ is reduced in ventricular myocytes in Akita mice (34) and PI3Kα knockout mice (35) (an effect that would presumably lead to APD shortening), which is different from our observations in Akita atrial myocytes. Collectively, our study demonstrates that the changes in AP morphology (especially V_{max}) and underlying ionic currents are different in the atria and ventricles in Akita mice and provides important insight into the distinct pattern of ion channel remodeling that occurs in the atria in Akita mice. Further work will be required to determine the basis for differences in atrial and ventricular electrophysiology in type 1 DM.

Chronic insulin treatment substantially reduced AF inducibility and burden and prevented changes in P-wave duration in Akita mice. Furthermore, acute application of insulin reduced the median duration of AF and shortened atrial P-wave duration. These findings suggest an important role for insulin signaling in the pathophysiology of AF in type 1 DM and indicate that this involves atrial electrical remodeling via both acute and chronic effects. In agreement with this, our studies also reveal a previously unknown role for insulin in regulating atrial I_{Na} in type 1 DM. We found that a major determinant of reduced I_{Na} in the atria of Akita mice was the reduction in atrial expression of *SCN5a* and $Na_V1.5$. Chronic insulin treatment prevented the declines in atrial I_{Na} density and $Na_V1.5$ protein levels, indicating that insulin plays an important role in the de novo synthesis of new $Na_V1.5$ channels due to changes in gene expression. Consistent with this, previous studies have shown that activation of PI3Kα up-regulates the expression of cardiac Na^+ channels (36–38).

Importantly, our investigations revealed additional effects of insulin that could be activated acutely (i.e., on the order of minutes). Specifically, acute insulin injection immediately prior to cell isolation or dialysis of atrial myocytes with PIP_3 each increased atrial I_{Na} by ~30%. Consistent with these results, acute insulin also shortened P-wave duration. As these effects were rapid, we infer that they do not involve changes in gene or protein expression. Rather, these results demonstrate that an important component of the effects of insulin are mediated by the acute activation of PIP_3 signaling via PI3K.

In addition to the effects of insulin on atrial I_{Na}, we found that inhibition of PKC also increases atrial I_{Na} (~38%) in association with a shift in $V_{1/2(act)}$ to values very similar to those measured in wild-type mice. This indicates that PKC activity is increased in the atria in Akita mice and that this can account for the change in I_{Na} activation kinetics. Consistent with this, PKC is known to be an important regulator of I_{Na} (29, 39), and previous studies have shown that PKCα expression is elevated in the heart in Akita mice (28). Thus, our studies demonstrate that atrial I_{Na} is reduced in Akita mice in association with both the loss of insulin signaling and enhanced PKC activity. The reductions in I_{Na} and AP V_{max} in the atria in Akita mice are likely major contributors to the increased susceptibility to AF in type 1 DM. These alterations can explain the impairments in atrial conduction and would be expected to be proarrhythmic by decreasing the wavelength of reentry (15, 40). This would favor of the occurrence and maintenance of AF and is consistent with AF being longer lasting in Akita mice.

Neither insulin or PIP_3 had any effect on the reduction in repolarizing I_K in Akita atrial myocytes, and APD remained prolonged. A reduction in $K_V1.5$ is known to contribute to atrial electrical remodeling in human chronic AF (41), and our findings indicate this may be the case in Akita diabetic mice as well. Prolongation of the APD in Akita atrial myocytes could contribute to the increased susceptibility to AF by increasing the likelihood of triggered activity in the form of EADs (15); however, we did not observe EADs in our studies, suggesting that this is not a major determinant of AF in Akita mice. Consistent with this, our data demonstrate that chronic insulin treatment reduced AF susceptibility and severity in association with improved atrial conduction, V_{max}, and I_{Na}, suggesting that these are critical for decreasing the inducibility of AF despite the lack of improvement in I_K or APD. Nevertheless, it is also possible that AP prolongation could contribute to impairments in atrial conduction in Akita mice either by contributing to the slowing of conduction at fast atrial rates or increasing the likelihood of conduction block. Additional studies will be required to determine how impaired atrial repolarization contributes to the slowing of atrial conduction and whether preventing AP prolongation can also reduce the susceptibility to AF in type 1 DM.

In addition to electrical remodeling, DM is also associated with structural remodeling due to atrial fibrosis. This has been demonstrated in human DM and in animal models (42–46). Indeed, we have previously demonstrated enhanced atrial fibrosis in the right and left atria in Akita mice (31). Fibrosis can also contribute to a substrate for AF since increased collagen deposition can impede atrial conduction and cause fragmentation of propagating wave fronts, thereby leading to reentry (15, 47–49). We have previously demonstrated that chronic insulin treatment reduces atrial fibrosis in Akita mice (31), and similar findings have been reported in STZ-injected rats treated with insulin (50). Thus, our prior work in combination with our present study demonstrates that insulin can prevent two alterations that are recognized as key contributors to impaired atrial conduction and maintenance of AF—the reduction in V_{max} due to reduced I_{Na} as well as increased atrial fibrosis—highlighting a previously unappreciated and important role for insulin as an antiarrhythmic agent for AF in type 1 DM. Consistent with these observations, it has been previously demonstrated that enhancing PI3Kα (activated downstream of the insulin receptor) can mitigate ventricular electrical remodeling in hypertrophy and heart failure (51, 52) and that reduced PI3Kα activity increases susceptibility to AF (53). Our data suggest that insulin must be delivered for timeframes that are adequate to increase the expression of $Na_V1.5$ and reduce fibrosis in order to maximize its protective effects on atrial electrical and structural remodeling in type 1 DM. While the acute activation of insulin signaling ($PI3K/PIP_3$ dependent) does increase atrial I_{Na}, and partially prevents P-wave prolongation, this was not sufficient by itself to fully reduce the AF burden or the prolongation in P-wave duration in vivo.

Some limitations of our study should be acknowledged. Our study was conducted in mice, which exhibit differences in the relative importance of some repolarizing I_K compared with humans. Specifically, the rapid and slow delayed rectifier K^+ currents (I_{Kr} and I_{Ks}), which are important in the human heart, do not play a major functional role in the mouse heart (18). Prior studies have shown alterations in some of these K^+ currents in canine models of DM (54). Nevertheless, our study shows that I_{Kur} (carried by $K_V1.5$ channels) is a major I_K that was altered in the atria in Akita mice. $K_V1.5$ is an atrial-specific I_K in the human heart (18, 55). It will be insightful to explore the alterations that we have identified in large animal models, tissue samples from human diabetic patients, or possibly, stem cell-derived atrial myocytes. While our study has focused on key ion channels in the atria in type 1 DM, it is possible that there are other alterations in gene and protein expression that are sensitive to insulin regulation. This could be explored in future studies using RNA sequencing. While we did not observe any changes in the mRNA levels of atrial connexins, it is possible that other aspects of connexin function or regulation could be altered in the atria in type 1 diabetes. Similarly, we did not observe changes in atrial calcium transient morphology in Akita mice; however, other aspects of calcium homeostasis could be altered in type 1 diabetes, which could potentially play a role in triggering AF in diabetes: for example, by delayed afterdepolarizations. Based on our findings, it will be important to conduct further studies to examine the links between glycemic control,

atrial conduction patterns, and AF occurrence in human diabetic patients. Finally, it will also be important to explore the effects of insulin or of enhancing insulin signaling via PI3K and PIP_3 in type 2 DM to determine if similar alterations and effects are present in this condition.

In conclusion, our study provides mechanistic insight into the cellular and molecular basis for AF in type 1 DM. This work demonstrates that AF in this setting is associated with electrical remodeling and changes in AP morphology due to reductions in atrial I_{Na} and $K_V1.5$-mediated repolarizing I_K. Furthermore, we have discovered that the reduction in I_{Na} is multifactorial, involving distinct acute and chronic effects of insulin as well as enhanced PKC activity. Finally, we show that insulin treatment is antiarrhythmic in type 1 DM via effects on atrial Na^+ channels but not K^+ channels. These data indicate that AF in type 1 DM has distinct features associated with the loss of normal insulin signaling. These findings have important implications for the treatment of AF in type 1 diabetic patients.

Materials and Methods

An expanded methods section is available in *SI Appendix*.

Mice. This study used male littermate wild-type and type 1 diabetic Akita mice between the ages of 16 and 22 wk. In some instances, male wild-type mice (16 to 18 wk) were treated with STZ (50 mg/kg intraperitoneal injection) to induce type 1 DM (56). The diabetic phenotype was confirmed by urinalysis to assess urine glucose (using keto-diastix reagent strips) as well as by measuring serum glucose levels (using a glucometer).

In chronic insulin treatment experiments, Akita mice were given insulin pellets (0.2 U/d per pellet) or placebo pellets (LinShin Canada Inc.) subcutaneously for 4 wk beginning at 12 wk of age. For acute insulin studies, Akita mice were given an intraperitoneal injection of insulin (5 to 10 U/kg) or saline, and 30 to 45 min later (after blood glucose was reduced), the mice were used experimentally.

All experimental procedures were approved by the University of Calgary Animal Care and Use Committee and the Dalhousie University Committee for Laboratory Animals and were in accordance with guidelines of the Canadian Council on Animal Care.

Echocardiography and Electrolyte Measurements. Cardiac structure and function were assessed by echocardiography in mice anesthetized by isoflurane inhalation (2%) using a Vevo 3100 ultrasound machine (Fujifilm VisualSonics) as we have described previously (21). Blood electrolytes were measured using an ePoc blood glass and electrolyte analyzer using blood samples drawn from the jugular vein.

In Vivo Electrophysiology. Surface electrocardiograms (ECGs) were measured in anesthetized mice (2% isoflurane inhalation) using 30-gauge subdermal needle electrodes (Grass Technologies). In conjunction, a 1.2F octapolar electrophysiology catheter (Transonic) was inserted into the right heart via an incision in the jugular vein and used to assess inducibility of AF during burst pacing as we have done previously (57, 58). Burst pacing protocols were standardized so that all mice were stimulated in identical fashion using the same pacing protocols. AF was defined as a rapid and irregular atrial rhythm (fibrillatory baseline in the ECG) with irregular R wave to R wave (RR) intervals lasting at least 1 s on the surface ECG and rapid irregular activity on the intracardiac atrial electrogram. AF was categorized into three groups: <5 s (brief), 5 to 30 s (nonsustained), and >30 s (sustained). Additional details are available in *SI Appendix*.

High-Resolution Optical Mapping. To study activation patterns and electrical conduction in the atria, high-resolution optical mapping was performed in isolated atrial preparations using methods that we have described in detail previously (31, 57, 59, 60). These atrial preparations were studied while in intrinsic sinus rhythm. Atrial preparations were immobilized using blebbistatin (10 μM) (61). Changes in fluorescence were captured using the voltage-sensitive dye Di-4-ANEPPS (10 μM) and a high-speed electron multiplying charge-coupled device camera at $\sim$900 frames per 1 s. Spatial resolution was 67 $\times$ 67 μM per pixel. Conduction velocity was measured locally in the right and left atria using approaches described previously (21, 22, 57, 58). In some instances, optical APs were measured by measuring the change in fluorescence as a function of time at individual pixels in the right and left atria as previously described (21, 22). All experiments were performed at 35 °C. Data were analyzed using custom software written in Matlab. Further details are available in *SI Appendix*.

Patch Clamping of Isolated Atrial Myocytes. Right and left atrial myocytes were isolated from mice by enzymatic digestion as we have described previously (62, 63). These myocytes were used to record APs using the perforated patch-clamp technique or the whole-cell patch-clamp technique (so that compounds could be dialyzed into the cells). AP parameters analyzed include resting membrane potential, V_{max}, overshoot, and APD. V_{max} was measured as the maximum rate of rise of the AP potential (i.e., dV/dt_{max}) between the resting membrane potential and the peak of the AP. I_{Na}, $I_{Na,L}$, I_K, and $I_{Ca,L}$ were recorded using the whole-cell patch-clamp technique. The solutions and experimental protocols for each of these approaches are available in *SI Appendix*.

qPCR. Quantitative gene expression was measured in the right and left atria as we have previously described (21, 22). Intron-spanning primers for *SCN5a* ($Na_V1.5$), *KCNA5* ($K_V1.5$), *GJA5* (Cx40), and *GJA1* (Cx43) as well as glyceraldehyde 3-phosphate dehydrogenase (GAPDH) (reference gene) were used. Experimental protocols and primer sequences are in *SI Appendix*.

Western Blotting. For western blotting, right and left atrial samples were used to measure the protein expression of $Na_V1.5$, $K_V4.2$, $K_V4.3$, and $K_V1.5$ as well as GAPDH as the loading control. The procedures for these experiments are provided in *SI Appendix*.

Calcium Transients. Calcium transients were measured using confocal imaging in acutely isolated atrial myocytes. The solutions and experimental protocols are provided in *SI Appendix*.

Statistical Analysis. All data are presented as means $\pm$ SEM. Data were analyzed using Fisher's exact test, Student's *t* test, two-way ANOVA with Tukey's post hoc test, or two-way repeated measures ANOVA with Tukey's post hoc test as indicated in each figure. $P < 0.05$ was considered significant.

Data Availability. Relevant data and associated experimental protocols required for interpreting conclusions are included in the manuscript and the *SI Appendix*. Any additional information, data, or experimental reagents are available from the corresponding author upon request.

ACKNOWLEDGMENTS. This work was supported by Canadian Institutes of Health Research Operating Grants MOP 142486 and PJT 166105 (to R.A.R.). H.J.J. was the recipient of a Nova Scotia Graduate Scholarship and a Dalhousie Medical Research Foundation MacDonald Graduate Scholarship and holds a Killam Postdoctoral Fellowship. L.J.B. holds a Libin Cardiovascular Institute of Alberta Graduate Studentship. Y.L. holds a Canadian Institutes of Health Research Postdoctoral Fellowship. E.E.E. held a Heart and Stroke Foundation of Canada Fellowship. R.A.R. held a New Investigator Award from the Heart and Stroke Foundation of Canada.

1. D. Dobrev, L. Carlsson, S. Nattel, Novel molecular targets for atrial fibrillation therapy. *Nat. Rev. Drug Discov.* **11**, 275–291 (2012).
2. S. Nattel, B. Burstein, D. Dobrev, Atrial remodeling and atrial fibrillation: Mechanisms and implications. *Circ Arrhythm Electrophysiol* **1**, 62–73 (2008).
3. J. Andrade, P. Khairy, D. Dobrev, S. Nattel, The clinical profile and pathophysiology of atrial fibrillation: Relationships among clinical features, epidemiology, and mechanisms. *Circ. Res.* **114**, 1453–1468 (2014).
4. S. Dahlqvist *et al.*, Risk of atrial fibrillation in people with type 1 diabetes compared with matched controls from the general population: A prospective case-control study. *Lancet Diabetes Endocrinol.* **5**, 799–807 (2017).
5. Y. Lin *et al.*, Mechanism of and therapeutic strategy for atrial fibrillation associated with diabetes mellitus. *ScientificWorld J.* **2013**, 209428 (2013).
6. A. R. Menezes *et al.*, Cardiometabolic risk factors and atrial fibrillation. *Rev. Cardiovasc. Med.* **14**, e73–e81 (2013).
7. L. J. Bohne *et al.*, The association between diabetes mellitus and atrial fibrillation: Clinical and mechanistic insights. *Front. Physiol.* **10**, 135 (2019).
8. Z. Xiong *et al.*, A machine learning aided systematic review and meta-analysis of the relative risk of atrial fibrillation in patients with diabetes mellitus. *Front. Physiol.* **9**, 835 (2018).
9. S. Dublin *et al.*, Diabetes mellitus, glycemic control, and risk of atrial fibrillation. *J. Gen. Intern. Med.* **25**, 853–858 (2010).
10. S. D. de Ferranti *et al.*, Type 1 diabetes mellitus and cardiovascular disease: A scientific statement from the American Heart Association and American Diabetes Association. *Circulation* **130**, 1110–1130 (2014).
11. E. D. Abel, Insulin signaling in heart muscle: Lessons from genetically engineered mouse models. *Curr. Hypertens. Rep.* **6**, 416–423 (2004).
12. G. Y. Oudit *et al.*, The role of phosphoinositide-3 kinase and pten in cardiovascular physiology and disease. *J. Mol. Cell. Cardiol.* **37**, 449–471 (2004).

13. B. Vanhaesebroeck, J. Guillermet-Guibert, M. Graupera, B. Bilanges, The emerging mechanisms of isoform-specific pi3k signalling. *Nat. Rev. Mol. Cell Biol.* **11**, 329–341 (2010).
14. B. Vanhaesebroeck, L. Stephens, P. Hawkins, Pi3k signalling: The path to discovery and understanding. *Nat. Rev. Mol. Cell Biol.* **13**, 195–203 (2012).
15. J. Heijman, N. Voigt, S. Nattel, D. Dobrev, Cellular and molecular electrophysiology of atrial fibrillation initiation, maintenance, and progression. *Circ. Res.* **114**, 1483–1499 (2014).
16. S. Nattel, Atrial electrophysiology and mechanisms of atrial fibrillation. *J. Cardiovasc. Pharmacol. Therapeut.* **8**(suppl. 1), S5–S11 (2003).
17. A. G. Kleber, Y. Rudy, Basic mechanisms of cardiac impulse propagation and associated arrhythmias. *Physiol. Rev.* **84**, 431–488 (2004).
18. J. M. Nerbonne, R. S. Kass, Molecular physiology of cardiac repolarization. *Physiol. Rev.* **85**, 1205–1253 (2005).
19. W. Hsueh *et al.*, Recipes for creating animal models of diabetic cardiovascular disease. *Circ. Res.* **100**, 1415–1427 (2007).
20. M. Yoshioka, T. Kayo, T. Ikeda, A. Koizumi, A novel locus, mody4, distal to d7mit189 on chromosome 7 determines early-onset niddm in nonobese c57bl/6 (Akita) mutant mice. *Diabetes* **46**, 887–894 (1997).
21. H. J. Jansen *et al.*, Distinct patterns of atrial electrical and structural remodeling in angiotensin II mediated atrial fibrillation. *J. Mol. Cell. Cardiol.* **124**, 12–25 (2018).
22. H. J. Jansen *et al.*, Npr-c (natriuretic peptide receptor-c) modulates the progression of angiotensin II-mediated atrial fibrillation and atrial remodeling in mice. *Circ. Arrhythm Electrophysiol.* **12**, e006863 (2019).
23. M. Mackasey *et al.*, Natriuretic peptide receptor-c protects against angiotensin II-mediated sinoatrial node disease in mice. *JACC Basic Transl. Sci.* **3**, 824–843 (2018).
24. H. Bugger *et al.*, Type 1 diabetic Akita mouse hearts are insulin sensitive but manifest structurally abnormal mitochondria that remain coupled despite increased uncoupling protein 3. *Diabetes* **57**, 2924–2932 (2008).
25. H. C. Kuo *et al.*, A defect in the Kv channel-interacting protein 2 (kchip2) gene leads to a complete loss of i(to) and confers susceptibility to ventricular tachycardia. *Cell* **107**, 801–813 (2001).
26. A. E. Lomax, C. S. Kondo, W. R. Giles, Comparison of time- and voltage-dependent K+ currents in myocytes from left and right atria of adult mice. *Am. J. Physiol. Heart Circ. Physiol.* **285**, H1837–H1848 (2003).
27. C. Fiset, R. B. Clark, T. S. Larsen, W. R. Giles, A rapidly activating sustained K+ current modulates repolarization and excitation-contraction coupling in adult mouse ventricle. *J. Physiol.* **504**, 557–563 (1997).
28. V. B. Patel *et al.*, Loss of angiotensin-converting enzyme-2 exacerbates diabetic cardiovascular complications and leads to systolic and vascular dysfunction: A critical role of the angiotensin II/at1 receptor axis. *Circ. Res.* **110**, 1322–1335 (2012).
29. C. Marionneau, H. Abriel, Regulation of the cardiac Na+ channel nav1.5 by post-translational modifications. *J. Mol. Cell. Cardiol.* **82**, 36–47 (2015).
30. D. Toullec *et al.*, The bisindolylmaleimide gf 109203x is a potent and selective inhibitor of protein kinase C. *J. Biol. Chem.* **266**, 15771–15781 (1991).
31. P. S. Krishnaswamy *et al.*, Altered parasympathetic nervous system regulation of the sinoatrial node in Akita diabetic mice. *J. Mol. Cell. Cardiol.* **82**, 125–135 (2015).
32. C. L. Stables *et al.*, Reduced Na(+) current density underlies impaired propagation in the diabetic rabbit ventricle. *J. Mol. Cell. Cardiol.* **69**, 24–31 (2014).
33. Z. Lu *et al.*, Increased persistent sodium current due to decreased pi3k signaling contributes to qt prolongation in the diabetic heart. *Diabetes* **62**, 4257–4265 (2013).
34. Z. Lu *et al.*, Decreased l-type Ca2+ current in cardiac myocytes of type 1 diabetic Akita mice due to reduced phosphatidylinositol 3-kinase signaling. *Diabetes* **56**, 2780–2789 (2007).
35. Z. Lu *et al.*, Loss of cardiac phosphoinositide 3-kinase p110 alpha results in contractile dysfunction. *Circulation* **120**, 318–325 (2009).
36. L. M. Ballou, R. Z. Lin, I. S. Cohen, Control of cardiac repolarization by phosphoinositide 3-kinase signaling to ion channels. *Circ. Res.* **116**, 127–137 (2015).
37. K. Kaur *et al.*, Tgf-beta1, released by myofibroblasts, differentially regulates transcription and function of sodium and potassium channels in adult rat ventricular myocytes. *PLoS One* **8**, e55391 (2013).
38. K. C. Yang, Y. T. Tseng, J. M. Nerbonne, Exercise training and pi3kalpha-induced electrical remodeling is independent of cellular hypertrophy and AKT signaling. *J. Mol. Cell. Cardiol.* **53**, 532–541 (2012).
39. J. Brouillette, R. B. Clark, W. R. Giles, C. Fiset, Functional properties of K+ currents in adult mouse ventricular myocytes. *J. Physiol.* **559**, 777–798 (2004).
40. S. Nattel, New ideas about atrial fibrillation 50 years on. *Nature* **415**, 219–226 (2002).
41. D. R. Van Wagoner *et al.*, Outward K+ current densities and kv1.5 expression are reduced in chronic human atrial fibrillation. *Circ. Res.* **80**, 772–781 (1997).
42. T. Kato *et al.*, Ages-rage system mediates atrial structural remodeling in the diabetic rat. *J. Cardiovasc. Electrophysiol.* **19**, 415–420 (2008).
43. T. Kato *et al.*, Angiotensin II type 1 receptor blocker attenuates diabetes-induced atrial structural remodeling. *J. Cardiol.* **58**, 131–136 (2011).
44. R. R. Lamberts *et al.*, Impaired relaxation despite upregulated calcium-handling protein atrial myocardium from type 2 diabetic patients with preserved ejection fraction. *Cardiovasc. Diabetol.* **13**, 72 (2014).
45. B. Li, Y. Pan, X. Li, Type 2 diabetes induces prolonged p-wave duration without left atrial enlargement. *J. Kor. Med. Sci.* **31**, 525–534 (2016).
46. M. Watanabe *et al.*, Conduction and refractory disorders in the diabetic atrium. *Am. J. Physiol. Heart Circ. Physiol.* **303**, H86–H95 (2012).
47. M. S. Dzeshka, G. Y. Lip, V. Snezhitskiy, E. Shantsila, Cardiac fibrosis in patients with atrial fibrillation: Mechanisms and clinical implications. *J. Am. Coll. Cardiol.* **66**, 943–959 (2015).
48. S. Rohr, Myofibroblasts in diseased hearts: New players in cardiac arrhythmias?. *Heart Rhythm* **6**, 848–856 (2009).
49. R. M. Wolf *et al.*, Atrial fibrillation and sinus node dysfunction in human ankyrin-b syndrome: A computational analysis. *Am. J. Physiol. Heart Circ. Physiol.* **304**, H1253–H1266 (2013).
50. S. Saito *et al.*, Glucose fluctuations increase the incidence of atrial fibrillation in diabetic rats. *Cardiovasc. Res.* **104**, 5–14 (2014).
51. K. C. Yang, P. Y. Jay, J. R. McMullen, J. M. Nerbonne, Enhanced cardiac pi3kalpha signalling mitigates arrhythmogenic electrical remodelling in pathological hypertrophy and heart failure. *Cardiovasc. Res.* **93**, 252–262 (2012).
52. K. C. Yang, Y. C. Ku, M. Lovett, J. M. Nerbonne, Combined deep microRNA and mRNA sequencing identifies protective transcriptomal signature of enhanced pi3kalpha signaling in cardiac hypertrophy. *J. Mol. Cell. Cardiol.* **53**, 101–112 (2012).
53. L. Pretorius *et al.*, Reduced phosphoinositide 3-kinase (p110alpha) activation increases the susceptibility to atrial fibrillation. *Am. J. Pathol.* **175**, 998–1009 (2009).
54. C. Lengyel *et al.*, Diabetes mellitus attenuates the repolarization reserve in mammalian heart. *Cardiovasc. Res.* **73**, 512–520 (2007).
55. D. Fedida *et al.*, Kv1.5 is an important component of repolarizing K+ current in canine atrial myocytes. *Circ. Res.* **93**, 744–751 (2003).
56. H. Bugger *et al.*, Genetic loss of insulin receptors worsens cardiac efficiency in diabetes. *J. Mol. Cell. Cardiol.* **52**, 1019–1026 (2012).
57. E. E. Egom *et al.*, Impaired sinoatrial node function and increased susceptibility to atrial fibrillation in mice lacking natriuretic peptide receptor c. *J. Physiol.* **593**, 1127–1146 (2015).
58. H. J. Jansen *et al.*, Atrial structure, function and arrhythmogenesis in aged and frail mice. *Sci. Rep.* **7**, 44336 (2017).
59. J. Azer, R. Hua, P. S. Krishnaswamy, R. A. Rose, Effects of natriuretic peptides on electrical conduction in the sinoatrial node and atrial myocardium of the heart. *J. Physiol.* **592**, 1025–1045 (2014).
60. M. Moghtadaei *et al.*, The impacts of age and frailty on heart rate and sinoatrial node function. *J. Physiol.* **594**, 7105–7126 (2016).
61. V. V. Fedorov *et al.*, Application of blebbistatin as an excitation-contraction uncoupler for electrophysiologic study of rat and rabbit hearts. *Heart Rhythm* **4**, 619–626 (2007).
62. R. Hua *et al.*, Effects of wild-type and mutant forms of atrial natriuretic peptide on atrial electrophysiology and arrhythmogenesis. *Circ. Arrhythm Electrophysiol.* **8**, 1240–1254 (2015).
63. J. Springer *et al.*, The natriuretic peptides BNP and CNP increase heart rate and electrical conduction by stimulating ionic currents in the sinoatrial node and atrial myocardium following activation of guanylyl cyclase-linked natriuretic peptide receptors. *J. Mol. Cell. Cardiol.* **52**, 1122–1134 (2012).

Supplementary Information for

Loss of insulin signaling contributes to atrial fibrillation and atrial electrical remodeling in type I diabetes mellitus

Iuliia Polina, Hailey J. Jansen, Tiesong Li, Motahareh Moghtadaei, Loryn J. Bohne, Yingjie Liu, Pooja Krishnaswamy, Emmanuel E. Egom, Darrell D. Belke, Sara A. Rafferty, Martin Ezeani, Anne M. Gillis, Robert A. Rose

Robert Rose
robert.rose@ucalgary.ca

Supplemental Methods

Mice

Male littermate wildtype and type 1 diabetic Akita mice (1, 2) between the ages of 16 and 22 weeks were used in this study. At this age range, hyperglycemia has developed to a stable level (2, 3). Akita mice were initially obtained from the Jackson Laboratory (strain C57BL/6-*Ins2*^{Akita}/J) and then bred locally. This mouse contains a mutation in the insulin-2 (*Ins2*) gene, *Ins2*^{C96Y}, which results in severe pancreatic β cell dysfunction and development of the diabetic phenotype (4). Heterozygous Akita mice (diabetic) and littermate wildtypes were used in this study. The diabetic phenotype was determined by assessing urine glucose (using keto-diastix reagent strips for urinalysis) as well as serum glucose levels (using a glucometer).

In some experiments, male wildtype C57BL/6 mice were treated with streptozotocin (STZ) to induce Type 1 DM (4). For these studies, mice were fasted for 6 hrs and then given an injection of STZ (50 mg/kg; intraperitoneal), or vehicle control (citrate buffer), once a day for 5 consecutive days (5). STZ injected mice developed hyperglycemia and were used experimentally 6 weeks after STZ injections were completed. Mice were 16-18 weeks of age at the time of experimental use.

In some cases Akita mice were treated with chronically with insulin (or placebo) for 4 weeks beginning at 12 weeks of age. This was done by implanting insulin or placebo pellets

(LinShin Canada) subcutaneously (2). These pellets release 0.2 units of insulin/day. Mice were anesthetized by isoflurane inhalation (3%) and pellets were implanted via a small puncture in the skin according to the manufacturer's instructions. Blood glucose was monitored in these animals before pellet implantation and then every 3 days after treatment began until the animals were used experimentally at 16 weeks of age. In other studies Akita mice were given acute intraperitoneal injections of insulin (5-10 U/kg), or saline as a control. 30-45 min later blood glucose was measured to ensure it was reduced and then the mice with used experimentally. In experiments in which atrial myocytes were isolated from mice acutely injected with insulin, these cells were used experimentally within 2 hours of isolation.

In vivo electrophysiology

Mice were anesthetized by isoflurane inhalation and subdermal needle electrodes (30 gauge) were placed around the heart in a lead II conformation. Surface ECG recordings were used to measure standard ECG parameters including RR interval, P wave duration, and PR interval.

A 1.2 French octapolar electrophysiology catheter containing 8 electrodes spaced 0.5 mm apart was used for intracardiac pacing experiments as we have described previously (6, 7). Inducibility of AF was studied using burst pacing in the right atrium (6, 7). We used 3 trains of 2 s burst pacing as follows: the first 2 s burst was given at a cycle length of 40 ms with a pulse duration of 5 ms. Following 3 min of stabilization a second 2 s burst was applied at a cycle length 20 ms with a pulse duration of 5 ms. After another 3 min of stabilization the final 2 s burst was given at a cycle length of 20 ms with a pulse duration of 10 ms. AF was defined as a rapid and irregular atrial rhythm (fibrillatory baseline in the ECG) with irregular RR intervals lasting at least 1 s on the surface ECG and the intracardiac atrial electrogram during any of the burst pacing protocols. All ECG data were acquired using a Gould ACQ-7700 amplifier and Ponemah

Physiology Platform software (Data Sciences International) as we have described previously (6, 7).

High resolution optical mapping

To study patterns of electrical conduction in the mouse atria we used high resolution optical mapping in atrial preparations as we (8) and others (9, 10) have done previously. To isolate our atrial preparation mice were administered a 0.2 ml intraperitoneal injection of heparin (1000 IU/ml) to prevent blood clotting and were then anesthetized by isoflurane inhalation and cervically dislocated. Hearts were excised into Krebs solution (35°C) containing (in mM): 118 NaCl, 4.7 KCl, 1.2 KH_2PO_4, 12.2 $MgSO_4$, 1 $CaCl_2$, 25 $NaHCO_3$, 11 glucose and bubbled with 95% O_2/5% CO_2 in order to maintain a pH of 7.4. The atria were dissected away from the ventricles and pinned in a dish with the epicardial surface facing upwards (towards the imaging equipment). The superior and inferior vena cavae were cut open so that the crista terminalis could be visualized and the preparation could be pinned out flat.

The atrial preparation was superfused continuously with Krebs solution (35°C) bubbled with 95% O_2/5% CO_2 and allowed to equilibrate for at least 30 min before data collection ensued. During this time the preparation was treated with the voltage sensitive dye di-4-ANEPPS (10 µM) for ~15 min and blebbistatin (10 µM) was added to the superfusate to suppress contractile activity (11, 12). Blebbistatin was present throughout the duration of the experiments in order prevent motion artifacts during optical mapping. Optical mapping studies were conducted on atrial preparation in sinus rhythm.

Di-4-ANEPPS loaded atrial preparations were illuminated with light at a wavelength of 520 – 570 nM using an EXFO X-cite fluorescent light source (Lumen Dynamics). Emitted light (590 – 640 nM) was captured using a high speed EMCCD camera (Evolve 128, Photometrics). Data were captured from an optical field of view of 8 x 8 mm^2 at a frame rate of ~900 frames/s

using Metamorph software (Molecular Devices). The spatial resolution was 67 x 67 µM for each pixel. Magnification was constant in all experiments and no pixel binning was used.

All optical data were analyzed using custom software written in Matlab. Pseudocolor electrical activation maps were generated from measurements of activation time at individual pixels as defined by assessment of dF/dt_{max}. In all cases background fluorescence was subtracted. Local conduction velocity (CV) was quantified specifically in the right atrial myocardium (within the RAA) and the left atrial myocardium (within the LAA) using an established approach previously described (8, 9, 13). Briefly, activation times at each pixel from a 7 x 7 pixel array were determined and fit to a plane using the least squares fit method. The direction on this plane that is increasing the fastest represents the direction that is perpendicular to the wavefront of electrical propagation and the maximum slope represents the inverse of the speed of conduction in that direction. With a spatial resolution of 67 x 67 µM per pixel, the area of the 7 x 7 pixel array was 469 x 469 µM. Five CV measurements were made in each region and averaged. Thus, using this method, we computed maximum local CV vectors in the atrial region of interest.

Isolation of mouse atrial myocytes

The procedures for isolating mouse atrial myocytes have been described previously (14, 15) and were as follows. Mice were administered a 0.2 ml intraperitoneal injection of heparin (1000 IU/ml) to prevent blood clotting. Following this, mice were anesthetized by isoflurane inhalation and then sacrificed by cervical dislocation. The heart was excised into Tyrode's solution (35ºC) consisting of (in mM) 140 NaCl, 5.4 KCl, 1.2 KH_2PO_4, 1.0 $MgCl_2$, 1.8 $CaCl_2$, 5.55 glucose, and 5 HEPES, with pH adjusted to 7.4 with NaOH. The right or left atrial appendage was dissected from the heart and cut into strips, which were transferred and rinsed in a 'low Ca^{2+}, Mg^{2+} free' solution containing (in mM) 140 NaCl, 5.4 KCl, 1.2 KH_2PO_4, 0.2 $CaCl_2$, 50 taurine, 18.5 glucose, 5 HEPES and 1 mg/ml bovine serum albumin (BSA), with pH adjusted to

6.9 with NaOH. Atrial tissue was digested in 5 ml of 'low Ca^{2+}, Mg^{2+} free' solution containing collagenase (type II, Worthington Biochemical Corporation), elastase (Worthington Biochemical Corporation) and protease (type XIV, Sigma Chemical Company) for 30 min. Then the tissue was transferred to 5 ml of modified KB solution containing (in mM) 100 potassium glutamate, 10 potassium aspartate, 25 KCl, 10 KH_2PO_4, 2 $MgSO_4$, 20 taurine, 5 creatine, 0.5 EGTA, 20 glucose, 5 HEPES, and 0.1% BSA, with pH adjusted to 7.2 with KOH. The tissue was mechanically agitated using a wide-bore pipette. This procedure yielded individual right or left atrial myocytes that were stored in KB solution until experimental use within 6 hours of isolation. Identical isolation procedures were used for wildtype and Akita mice and there were no discernable differences in cell yield or cell quality between groups during patch-clamp experiments.

Isolation of mouse ventricular myocytes

Mice were anesthetized by isoflurane inhalation and then euthanized by cervical dislocation. The heart was excised and retrogradely perfused with myocyte buffer (35°C) consisting of (in mM) 113 NaCl, 4.7 KCl, 1.2 $MgCl_2$, 0.6 KH_2PO_4, 0.6 NaH_2PO_4, 5 BDM (2,3-butanedione monoximine), 1.6 $NaHCO_3$, 30 taurine, 20 glucose, and 10 HEPES, with pH adjusted to 7.4 with NaOH. After the initial 2-3 minutes, the myocyte buffer was switched to digestion solution containing 0.1 mM $CaCl_2$, collagenase (type II, Worthington Biochemical Corporation) and protease (type XIV, Sigma Chemical Company) and the heart was perfused for 10-12 minutes at a flow rate of 1 ml/min. Finally, the heart was perfused with stopping buffer (myocyte buffer containing 2.5% bovine serum albumin and 0.1 mM $CaCl_2$) for another 2-3 minutes. After perfusion, the ventricles were excised and transferred to 5 ml of stopping buffer. The tissue was mechanically disaggregated using forceps and gently triturated with a 10 ml serological pipette. Then another 5 ml of fresh stopping buffer was added to bring the volume to

10 ml. $CaCl_2$ ws added to restore the Ca^{2+} concentration to 0.5 mM in four steps every 5 minutes.

Solutions and electrophysiological protocols

Stimulated action potentials (APs) were recorded using either the perforated patch-clamp technique or the whole cell patch-clamp technique. The latter was used to allow compounds to be dialyzed into cells via the patch pipette. There were no differences in AP parameters between perforated and whole cell configurations. To record APs the recording chamber was superfused with a normal Tyrode's solution (22 – 23ºC) containing (in mM) 140 NaCl, 5 KCl, 1 $MgCl_2$, 1 $CaCl_2$, 10 HEPES, and 5 glucose, with pH adjusted to 7.4 with NaOH. The pipette filling solution contained (in mM) 135 KCl, 0.1 $CaCl_2$, 1 $MgCl_2$, 5 NaCl, 10 EGTA, 4 Mg-ATP, 6.6 Na-phosphocreatine, 0.3 Na-GTP and 10 HEPES, with pH adjusted to 7.2 with KOH. Amphotericin B (200 µg/ml) was added to this pipette solution to record APs with the perforated patch clamp technique. APs were stimulated with a 20 ms depolarizing pulses of 0.6-0.7 nA.

For recording I_{Na} atrial myocytes were superfused with a modified Tyrode's solution (22 – 23°C) containing the following (in mM): 130 CsCl, 5 NaCl, 5.4 TEA-Cl, 1 $MgCl_2$, 1 $CaCl_2$, 10 HEPES, 5.5 glucose, (pH 7.4, adjusted with CsOH). Nitrendipine (10 µM) was added to the superfusate to block $I_{Ca,L}$. The pipette solution for I_{Na} contained (in mM): 120 CsCl, 5 NaCl, 1 $MgCl_2$, 0.2 $CaCl_2$, 10 HEPES, 5 MgATP, 0.3 Na-GTP, 5 BAPTA (pH 7.2, adjusted with CsOH). I_{Na} was recorded using 50 ms voltage clamp steps between -100 and 10 mV from a holding potential of -120 mV. I_{Na} activation kinetics were determined by calculating chord conductance (G) with the equation $G=I/(V_m-E_{rev})$, where V_m represents the depolarizing voltages and E_{rev} is the reversal potential estimated from the current-voltage relationships of $I_{Ca,L}$ or I_{Na}. Maximum conductance (G_{max}) and $V_{1/2}$ of activation for $I_{Ca,L}$ and I_{Na} were determined using the following function: $G=[(V_m-V_{rev})][G_{max}][-1/[(1+\exp((V_m-V_{1/2})/k))+1]]$. I_{Na} inactivation kinetics were measured

using 500 ms pre-pulse voltage clamp steps between -120 and -30 mV from a holding potential of -120 mV followed by a 20 ms test pulse to -20 mV. Normalized peak currents were plotted as a function of the pre-pulse potential and the resulting curve was fitted with the Boltzmann function $h=1/[1+\exp[V_{1/2}-V]/k]$. These data were used to measure the voltage at which 50% of channels are inactivated ($V_{1/2(act)}$).

Potassium currents (I_K) were recorded in the whole cell configuration using the normal Tyrode's solution and pipette solution as used to record APs. To record total potassium currents (no pre-pulse), cells were held at -80 mV then I_K was recorded using voltage clamp steps (500 ms duration) between -120 and +80 mV in 10 mV increments. To record potassium currents with an inactivating pre-pulse (to inactivate I_{to}), cells were given a 200 ms pre-pulse to -40 mV immediately followed by 500 ms voltage clamp steps from -120 to +80 mV from a holding potential of -80 mV. For these recordings with and without a pre-pulse recordings, I_K was measured at the peak current for each voltage step. I_{to} was calculated as the difference current between the recording with and without a pre-pulse (16, 17).

I_{Kur}, as carried by Kv1.5 channels, was measured as the component of I_K sensitive to 4-aminopyradie (4-AP; 100 µM) (16, 18). The voltage clamp protocol for measuring I_{Kur} included a pre-pulse to -40 mV for 200 ms to inactivate I_{to} immediately followed by a 500 ms step to +30 mV before returning to a holding potential of -80 mV. Peak currents at baseline, in the presence of 4-AP, and after washout were measured.

For recording $I_{Ca,L}$ atrial myocytes were superfused with a modified Tyrode's solution (22 – 23ºC) containing the following (in mM) 145 TEA-Cl, 2 $CaCl_2$, 1 $MgCl_2$, 10 HEPES, and 5 glucose with pH adjusted to 7.4 with NaOH. The pipette solution for $I_{Ca,L}$ contained (in mM) 135 CsCl, 0.1 $CaCl_2$, 1 $MgCl_2$, 5 NaCl, 10 EGTA, 4 Mg-ATP, 6.6 Na-phosphocreatine, 0.3 Na-GTP and 10 HEPES, with pH adjusted to 7.2 with CsOH. $I_{Ca,L}$ was recorded from a holding potential of -60 mV due to the expression of $Ca_V1.2$ and $Ca_V1.3$ in atrial myocytes (14, 15, 19, 20). Thus,

our voltage clamp protocols enable us to record total $I_{Ca,L}$, which could include contributions from $Ca_V1.2$ as well as $Ca_V1.3$.

For recording $I_{Na,L}$ atrial myocytes were superfused with a modified Tyrode's solution (22-23 ºC) containing the following (in mM): 135 NaCl, 5 TEA-Cl, 4 CsCl, 2 $MgCl_2$, 10 glucose, 10 HEPES, 0.03 niflumic acid, 0.004 strophanthidin, and 0.01 nifedipine with pH adjusted to 7.4 with NaOH. The pipette solution for $I_{Na,L}$ contained (in mM) 130 CsCl, 5 NaCl, 1 $MgCl_2$, 0.2 $CaCl_2$, 10 HEPES, 5 Mg-ATP, 0.3 Na-GTP, 10 EGTA with pH adjusted to 7.2 with CsOH. $I_{Na,L}$ was recorded using 1 s voltage clamp steps to -35 mV from a holding potential of -120 mV. $I_{Na,L}$ was measured as an integral from 100-150 ms after peak I_{Na}.

To study early afterdepolarization (EAD) susceptibility, APs were recorded at pacing frequencies of 2, 1, 0.2 and 0.1 Hz in baseline conditions and in the presence of 1 μM isoproterenol (ISO). A minimum of 30 APs were recorded in each condition and at each pacing frequency and examined for the occurrence of EADs.

Micropipettes were pulled from borosilicate glass (with filament, 1.5 mm OD, 0.75 mm ID, Sutter Instrument Company) using a Flaming/Brown pipette puller (model p-87, Sutter Instrument Company). The resistance of these pipettes was 4 – 8 MΩ when filled with recording solution. Micropipettes were positioned with a micromanipulator (Burleigh PCS-5000 system) mounted on the stage of an inverted microscope (Olympus IX71). Seal resistance was 2 – 15 GΩ. Rupturing the sarcolemma in the patch for voltage clamp experiments resulted in access resistances of 5 – 15 MΩ. Series resistance compensation averaged 80 – 85% using an Axopatch 200B amplifier (Molecular Devices). Capacitative currents were not subtracted from currents. Recorded signals were filtered with a 1 KHz low pass Bessel filter. For perforated patch clamp experiments access resistance was monitored for the development of capacitative transients upon sealing to the cell membrane with Amphotericin B in the pipette. Typically, access resistance became less than 25 MΩ within 5 min of sealing onto the cell, which was sufficient for recording stimulated APs in current clamp mode. Data were digitized using a

Digidata 1440 and pCLAMP 10 software (Molecular Devices) and stored on computer for analysis.

Quantitative PCR

Total RNA was isolated from right or left atrial appendages using a PureZOL™ RNA Isolation Reagent and the Aurum™ Total RNA Fatty and Fibrous Tissue Kit (Bio-Rad Laboratories) as per kit instructions. RNA samples were eluted from the spin column in 40 µL elution buffer. RNA yield and purity were assessed using a Nanodrop. All samples had a A_{260}/A_{280} of over 2.0 and therefore were free of DNA contamination. Next, cDNA (20 ng/µL) was synthesized using the iScript™ cDNA Synthesis Kit (Bio-Rad Laboratories). Reactions were performed in a Bio-Rad MyCycler thermal cycler using the following protocol: 5 min of priming at 25ºC followed by reverse transcription for 30 min at 42ºC then 5 min at 85ºC to inactivate reverse transcriptase.

All qPCR reactions were run in duplicate in 10 µL reactions that contained the following: 4 µL sample cDNA, 5.6 µL GoTaq® qPCR Master Mix (Promega), and 0.4 µL primers. Primers were reconstituted to a final concentration of 100 µM with nuclease free water and stored at -20ºC until use. Primers were diluted to 10 µM for qPCR reactions. RT-qPCR reactions were performed using the CFX386 Touch™ Real-Time PCR Detection System (Bio-Rad) using the following protocol: Taq polymerase was activated for 2 min at 95ºC followed by 39 cycles of denaturing for 15 s at 95ºC, annealing for 30 s at 60ºC, and extension for 30s at 72ºC. This was followed by melt curve analysis from 65-95ºC in 0.5ºC increments. Data were analyzed using the $2^{-\Delta\Delta C}{}_T$ method using the CFX Manager Software version 3.1 (Bio-Rad). Gene expression was normalized to GAPDH. Primer sequences are listed in Supplemental Table 17 below.

Western blotting

Atria were homogenized in an ice-cold RIPA buffer (50 mM Tris, 150 mM NaCl, 1 mM EDTA, 0.5% sodium Deoxycholic, 1% NP-40, 0.1% SDS) containing 2mM phenylmethane sulfonyl fluoride (Sigma), Halt™ Protease Inhibitor Cocktail (Thermo Fisher scientific). Preparations were centrifuged at 15000 rpm for 30 mins. Protein concentrations were measured using a Bio-Rad *DC*™ Protein Assay Kit II (Bio-Rad Laboratories). Protein samples (30 µg/lane) were separated by 7.5% SDS-polyacrylamide gels (SDS-PAGE) and transferred onto Immun-Blot® PVDF membrane (Bio-Rad). The membrane was blocked with 5% milk in Tris-buffer saline Tween-20 (TBST) for 1 hour and then incubated overnight at 4^0C with primary antibodies (Kv1.5 1:500, Kv4.2 1:500, Kv4.3 1:500, Nav1.5 1:500, all from Alomone Labs or GAPDH 1:2000, Abcam). The membrane was washed with TBST and then incubated with goat anti-rabbit IgG coupled to horseradish peroxidase (HRP) at 1:4000 for 1 hour at room temperature. ECL (Bio-Rad) was added and membrane was scanned using the ChemiDoc XRS+ system (Bio-Rad).

Calcium transients

Calcium transients were measured using confocal imaging in acutely isolated atrial myocytes. Right atrial myocytes were loaded with 5 µg/ml Rhod-2-AM for 15 minutes in a chamber pre-coated with 50 µg/ml R-laminin. After dye loading the cell chamber was washed to remove any excess dye by superfusing the myocytes with KRH buffer (125 mM NaCl, 5 mM KCl, 1.2 mM $MgCl_2$, 1.2 mM KH_2PO_4, 25 mM HEPES and 12 mM glucose, pH=7.4) containing 1mM $CaCl_2$ and then switched to KRH containing 1.8mM $CaCl_2$ and 5µM (S)-(-)-Blebbistatin. The myocytes were field stimulated (24 V) using a stimulation chamber (Warner Instruments) at 1 Hz. Recordings were obtained at 37°C using a Nikon confocal microscope with NIS-Elements AR software by performing line scans longitudinally along the cell membrane. Calcium transient morphology was analyzed using Clampfit. Paramters analyzed include the time to peak (T_{peak}) and time to 25%, 50%, 75% and 90% decay (T_{25}, T_{50}, T_{75} and T_{90}).

Supplemental Figures

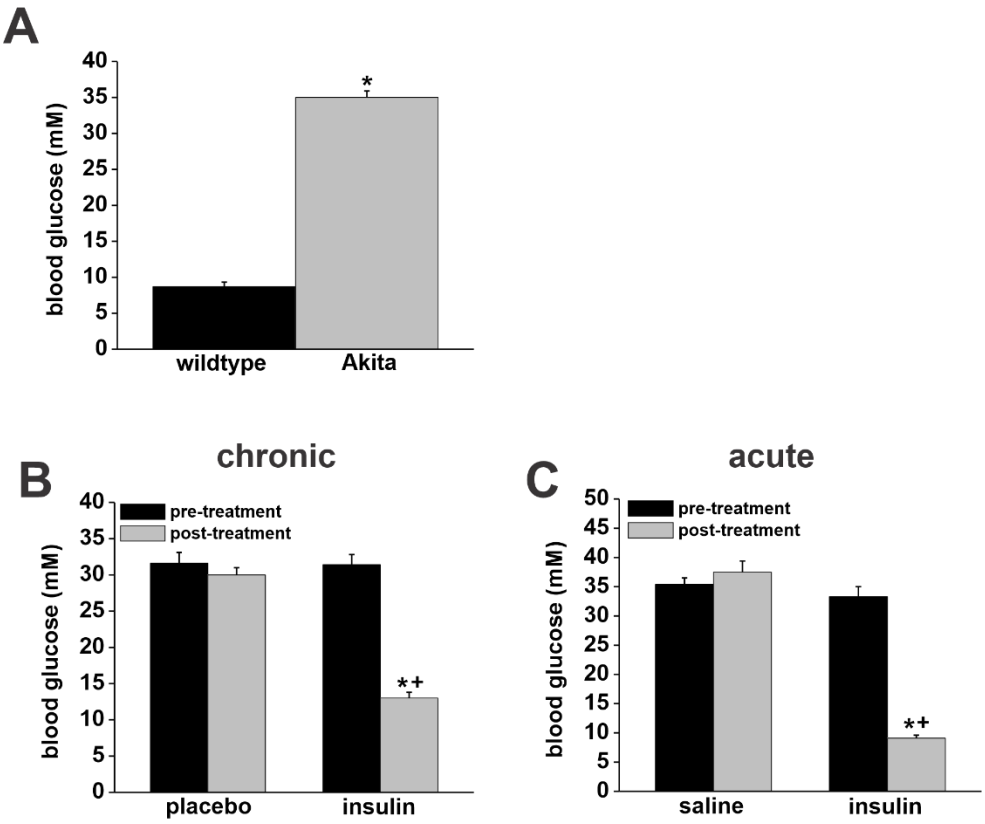

Figure S1. Blood glucose measurements. (*A*) Blood glucose values in wildtype and Akita mice. **P*<0.05 vs. wildtype by Student's *t*-test, *n*=22 wildtype and 27 Akita mice. (*B*) Blood glucose values in Akita mice at baseline (pre-treatment) and after 4 weeks of insulin treatment (post-treatment). **P*<0.05 vs. pre-treatment, ^{+}P<0.05 vs. saline by two-way ANOVA with Tukey's posthoc test, *n*=21 Akita mice for placebo and 24 for chronic insulin. (*C*) Blood glucose values in Akita mice at baseline (pre-treatment) and 30-45 min after injection with insulin (post-treatment). **P*<0.05 vs. pre-treatment, ^{+}P<0.05 vs. saline injection by two-way ANOVA with Tukey's posthoc test, *n*=11 Akita mice for saline and 16 for acute insulin.

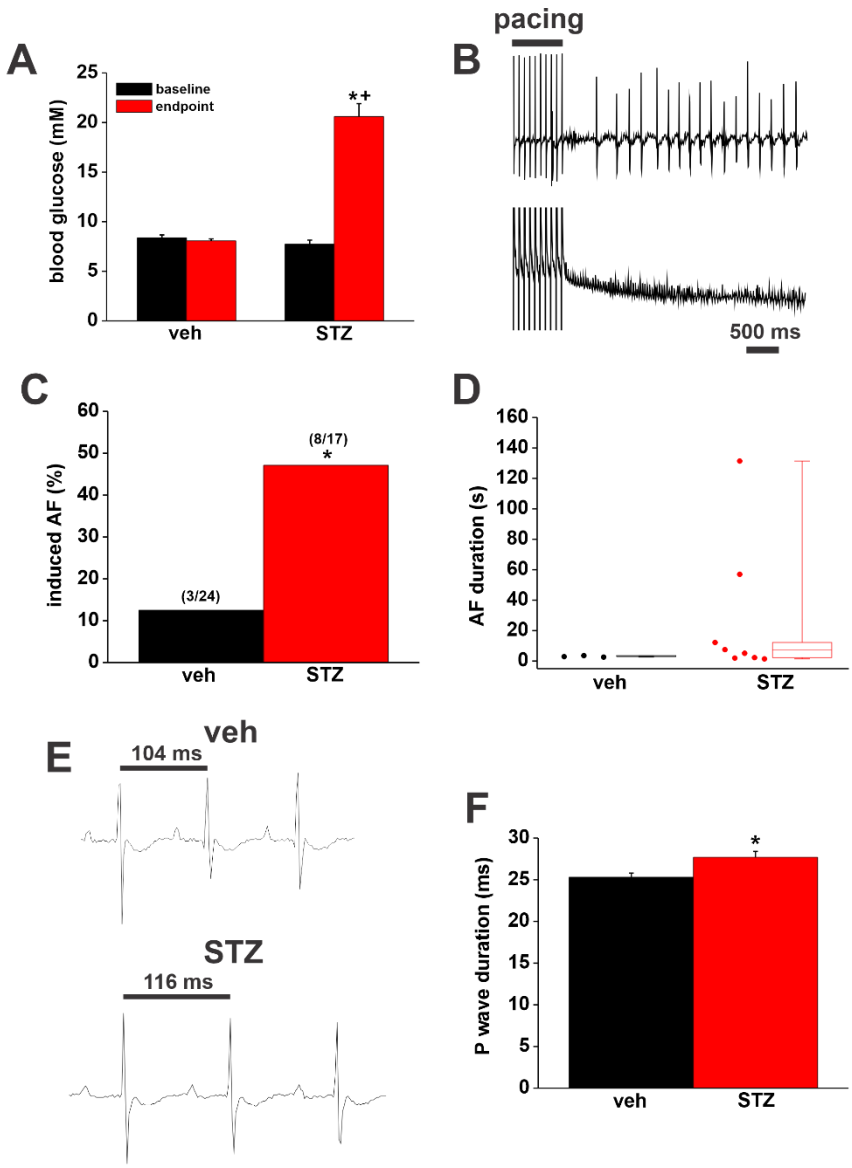

Figure S2. Atrial fibrillation and atrial electrophysiology in STZ injected diabetic mice. (*A*) blood glucose values at baseline and endpoint after STZ or vehicle (veh) injection. **P*<0.05 vs. baseline; $^{+}$*P*<0.05 vs. veh by two-way ANOVA with Tukey's posthoc test; *n*=24 veh and 17 STZ mice. (*B*) Representative surface (top) and intracardiac atrial (bottom) electrograms illustrating the induction of AF in an STZ treated mouse. (*C*) Susceptibility to induced AF in veh and STZ injected mice **P*<0.05 by Fischer's exact test. (*D*) Duration of AF in veh and STZ injected mice that were induced into AF. (*E*) Representative surface ECGs in veh and STZ injected mice. (*F*) Summary of P wave durations in veh and STZ injected mice. **P*<0.05 vs. veh by Student's *t*-test.

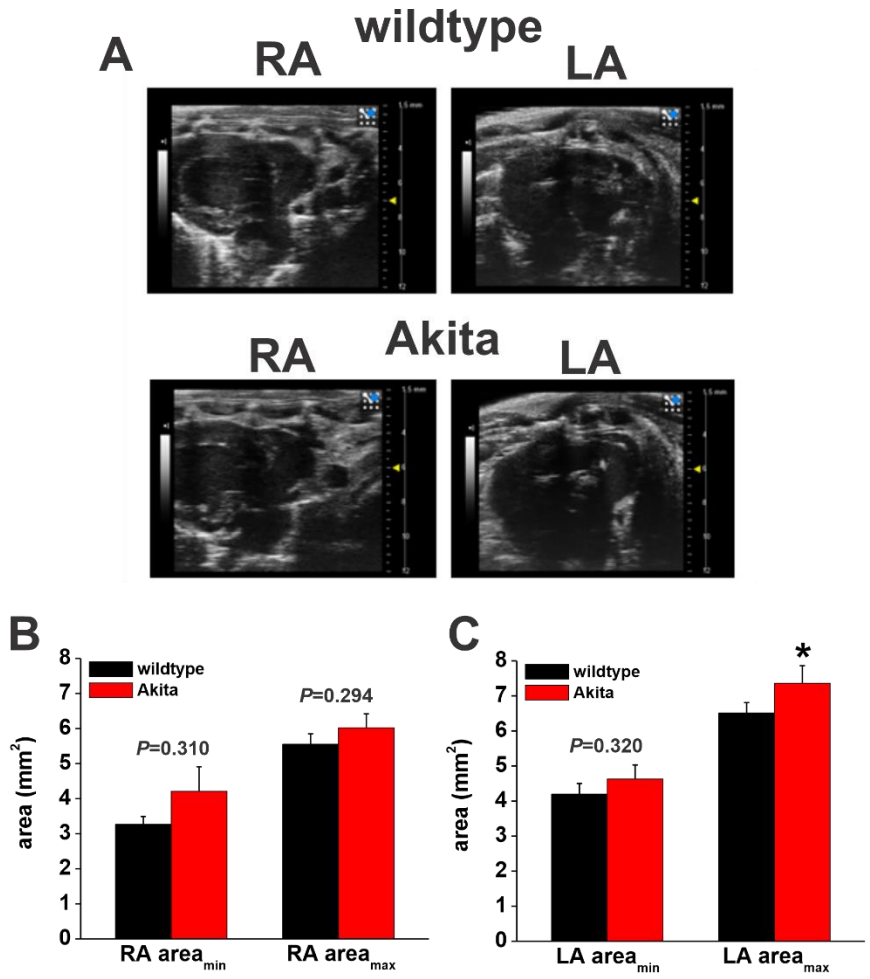

Figure S3. Echocardiography in Akita mice. (*A*) Representative images used to assess right atrial (RA) and left atrial (LA) area in wildtype and Akita mice. Bars on left side of images represent contrast intensity. Scale bars on right side of images are measures of distance (mm). (*B*) Minimum and maximum RA area in wildtype and Akita mice. (*C*) Minimum and maximum LA area in wildtype and Akita mice. **P*<0.05 vs. wildtype by two-way ANOVA with Tukey's posthoc test; *n*=11 mice per group. Refer to Table S9 for a summary of echocardiography analysis.

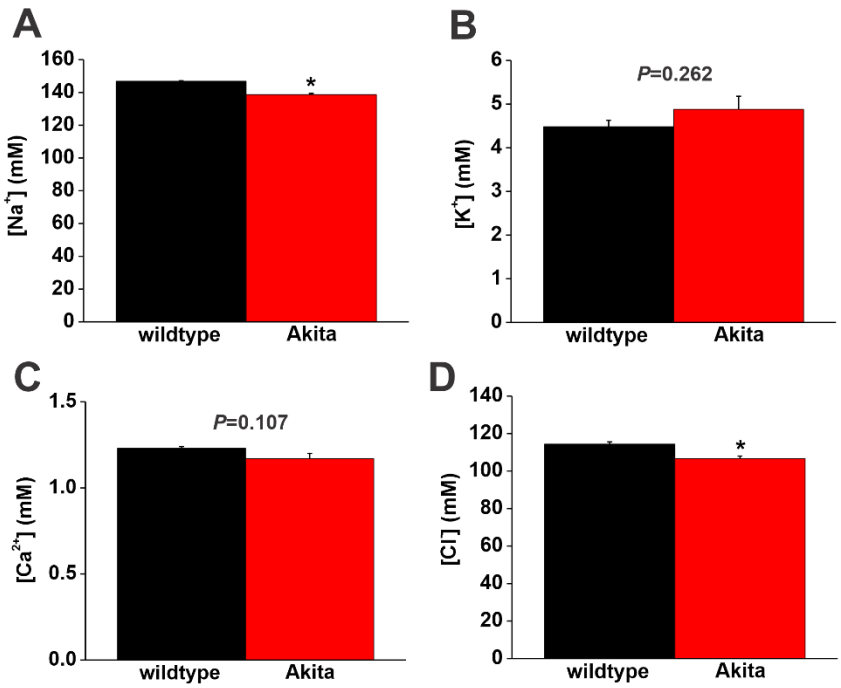

Figure S4. Blood electrolytes in Akita mice. Blood concentrations of Na^+ (*A*), K^+ (*B*), Ca^{2+} (*C*) and Cl^- (*D*) in wildtype and Akita mice. **P*<0.05 vs. wildtype by Student's *t*-test; *n*=6 mice per group.

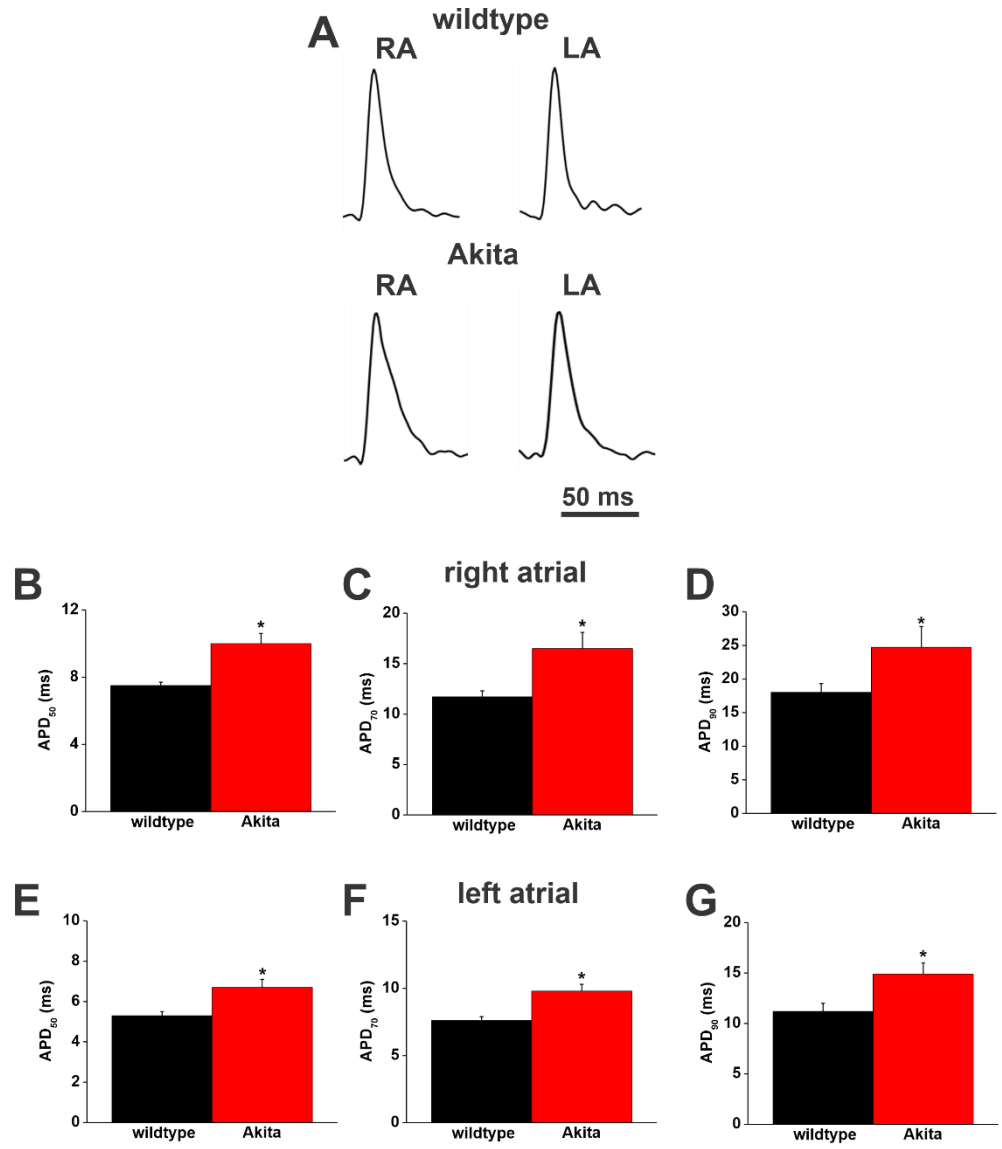

Figure S5: Optical action potential duration in wildtype and Akita mice. (*A*) Representative optical APs in right and left atria from wildtype and Akita mice. (*B-D*) Summary of right atrial APD_{50} (*B*), APD_{70} (*C*) and APD_{90} (*D*) for wildtype and Akita mice. (*E-G*) Summary of left atrial APD_{50} (*E*), APD_{70} (*F*), and APD_{90} (*G*). *$P<0.05$ vs. wildtype by Student's *t*-test; $n=5$ hearts per group.

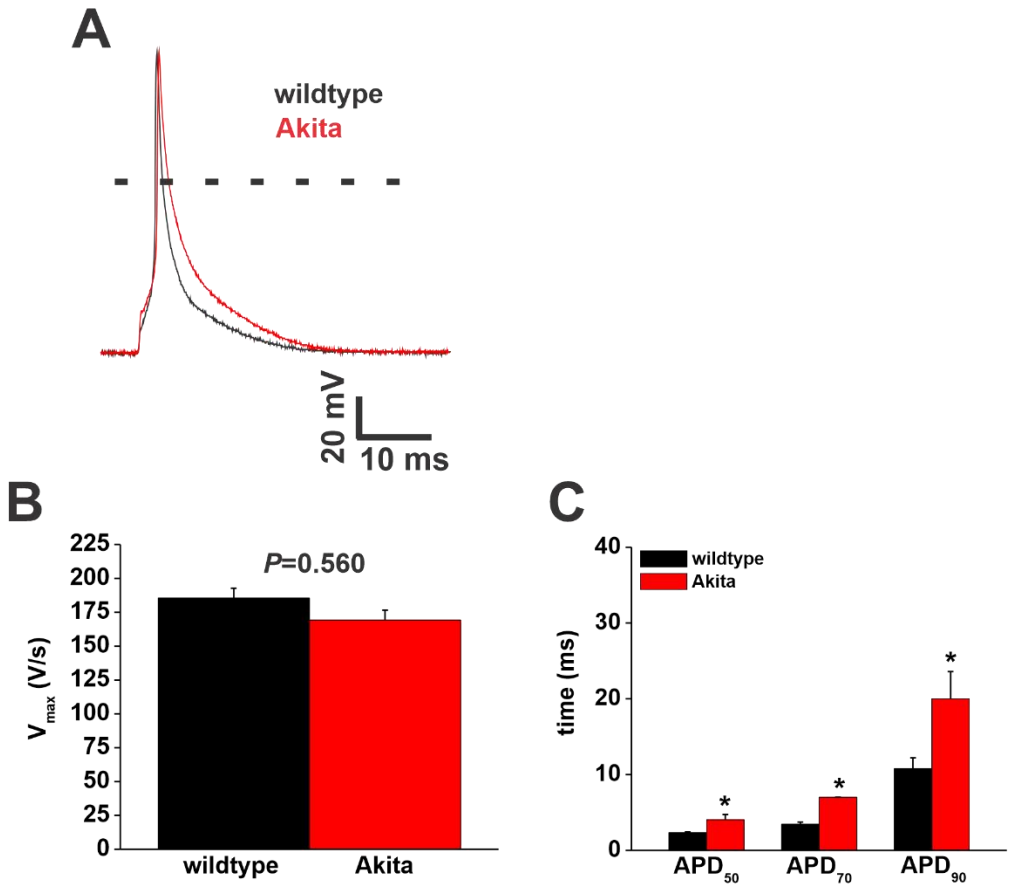

Figure S6: Ventricular myocyte action potential morphology in Akita mice. (*A*) Representative stimulated APs in isolated ventricular myocytes from wildtype and Akita mice. (*B*) AP V_{max} in isolated ventricular myocytes from wildtype and Akita mice. (*C*) AP duration at 50% (APD_{50}), 70% (APD_{70}) and 90% (APD_{90}) repolarization in wildtype and Akita mice. **P*<0.05 vs. wildtype by Student's *t*-test; *n*=8 for wildtype and 11 for Akita.

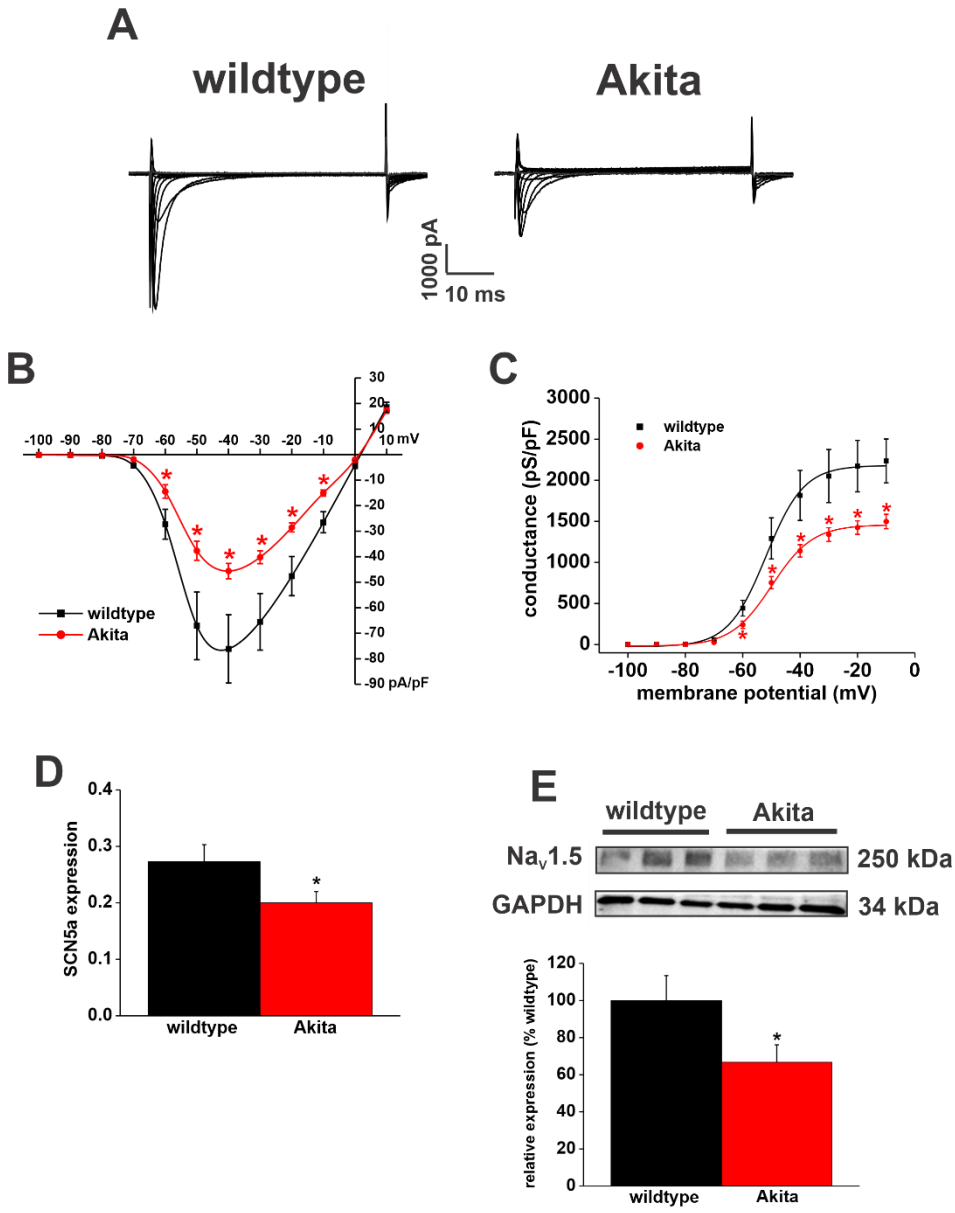

Figure S7. I_{Na} is reduced in left atrial myocytes in Akita mice. (*A*) Representative I_{Na} recordings in left atrial myocytes isolated from wildtype and Akita mice. Cell capacitances for these representative recordings was 42 pF for wildtype and 49 pF for Akita. (*B*) I_{Na} IV curves in left atrial myocytes isolated from wildtype and Akita mice. (*C*) I_{Na} activation curves in left atrial myocytes from wildtype and Akita mice. For left atrial myocytes n=5 for wildtype and 11 for Akita; *P<0.05 vs. wildtype at each membrane potential by two-way repeated measures ANOVA with Tukey's posthoc test. I_{Na} activation kinetics are summarized in Supplemental Table 13. (*D*) *SCN5a* gene expression in the right atrium in wildtype and Akita mice. *P<0.05 vs. wildtype by Student's t-test; n=15 wildtype and 17 Akita mice. (*E*) $Na_V1.5$ protein expression in the left atrium in wildtype and Akita mice. *P<0.05 vs. wildtype by Student's t-test, n=6 wildtype and 6 Akita mice.

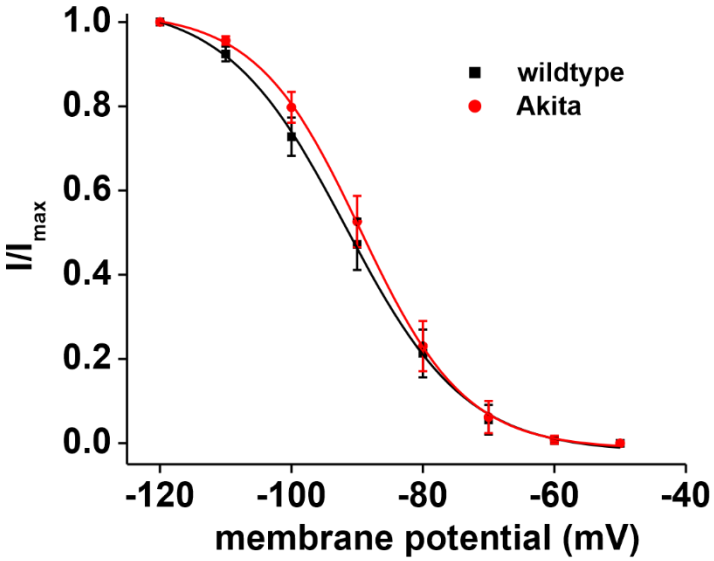

Figure S8: Steady state I_{Na} inactivation in Akita right atrial myocytes. I_{Na} inactivation curves for wildtype and Akita right atrial myocytes. There was no difference (*P*=0.341) in I_{Na} $V_{1/2(inact)}$ between wildtype (-91.3 ± 2.4 mV) and Akita (-88.9 ± 2.2 mV) mice. Data analyzed by Student's *t*-test; *n*=11 wildtype myocytes and 10 Akita myocytes.

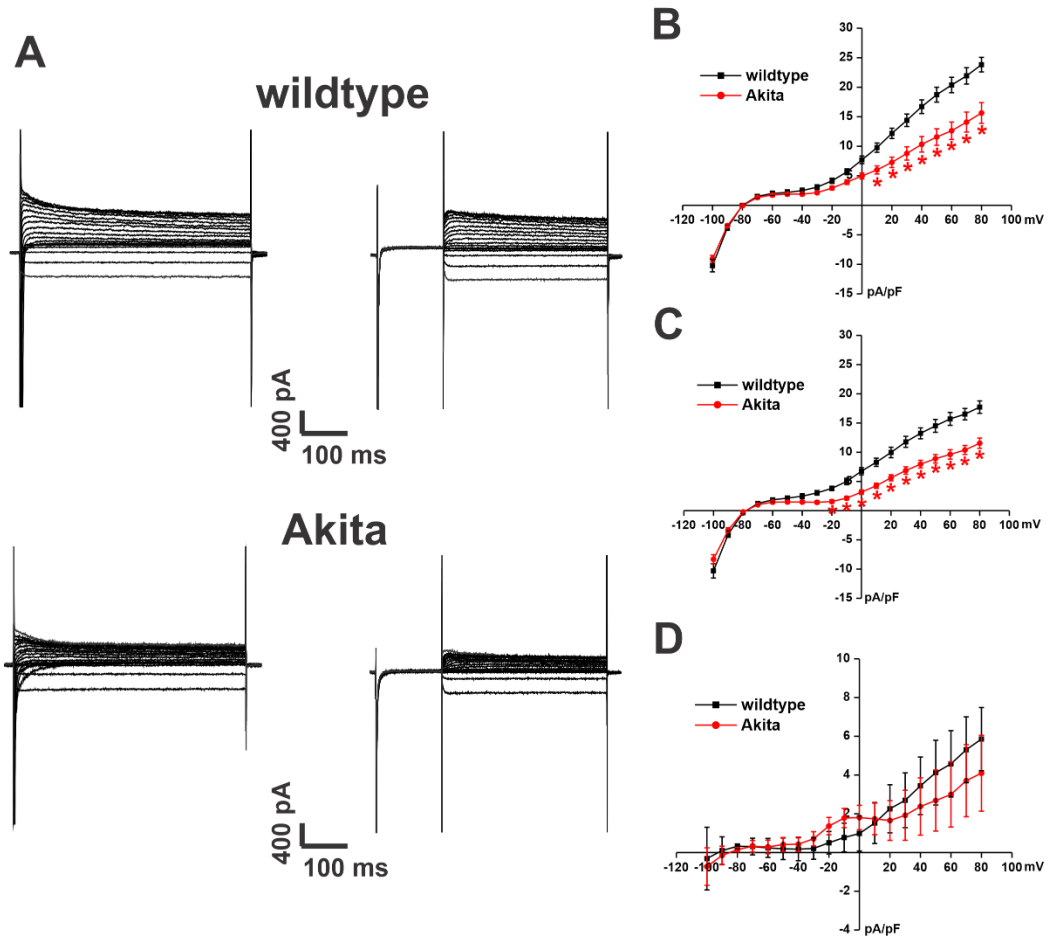

Figure S9. Repolarizing K^+ current is reduced in left atrial myocytes in Akita mice. (*A*) Representative K^+ current recordings in left atrial myocytes isolated from wildtype and Akita mice. The recordings on the left represent total I_K measured between -100 and +80 mV. The recordings on the right represent I_K measured between -100 and +80 mV following a pre-pulse to -40 mV to inactivate I_{to}. Cell capacitances for these representative recordings was 49 pF for wildtype and 43 pF for Akita. (*B*) I_K IV curves measured at the peak of the I_K recordings without the pre-pulse (recordings on the left in panel A) for left atrial myocytes isolated from wildtype and Akita mice. (*C*) I_K IV curves measured at the peak of the I_K recordings with the pre-pulse (recordings on the right in panel A) for left atrial myocytes isolated from wildtype and Akita mice. For panels *B* and *C* **P*<0.05 vs. wildtype at each membrane potential by two-way repeated measures ANOVA with Tukey's posthoc test. (*D*) I_K IV curves for the different current between *B* and *C*, which is a measure of I_{to}. There was no difference (*P*=0.73) in I_{to} density between wildtype and Akita. For panels *B*-*D* *n*=13 wildtype and 11 Akita left atrial myocytes.

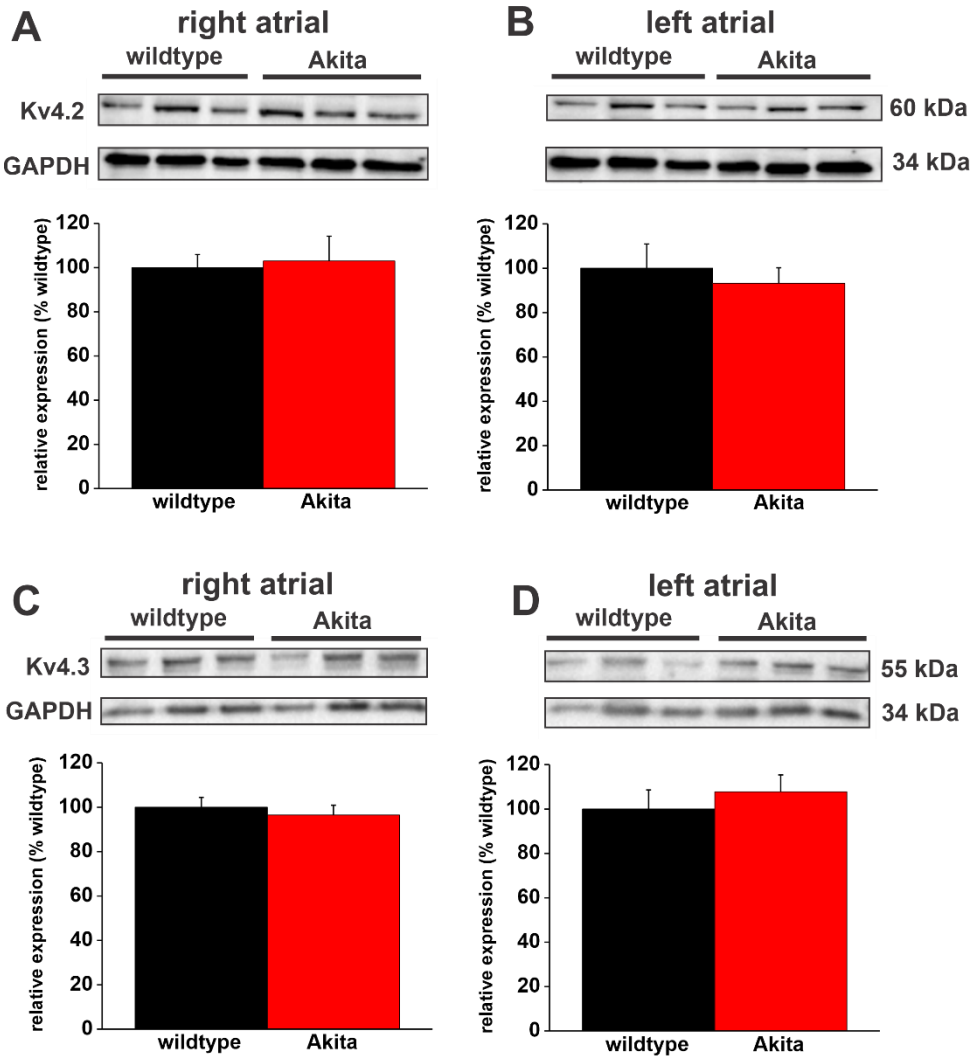

Figure S10. Protein expression of K_V4.2 and K_V4.3 in right and left atria. (*A*) Expression of K_V4.2 in the right atrium in wildtype and Akita mice. *P*=0.79 by Student's t-test, *n*=6 for wildtype and 6 for Akita. (*B*) Expression of K_V4.2 in the left atrium in wildtype and Akita mice. *P*=0.61 by Student's *t*-test, *n*=6 for wildtype and 6 for Akita. (*C*) Expression of K_V4.3 in the right atrium in wildtype and Akita mice. *P*=0.58 by Student's *t*-test, *n*=9 for wildtype and 9 for Akita. (*D*) Expression of K_V4.3 in the left atrium in wildtype and Akita mice. *P*=0.51 by Student's *t*-test, *n*=9 for wildtype and 9 for Akita.

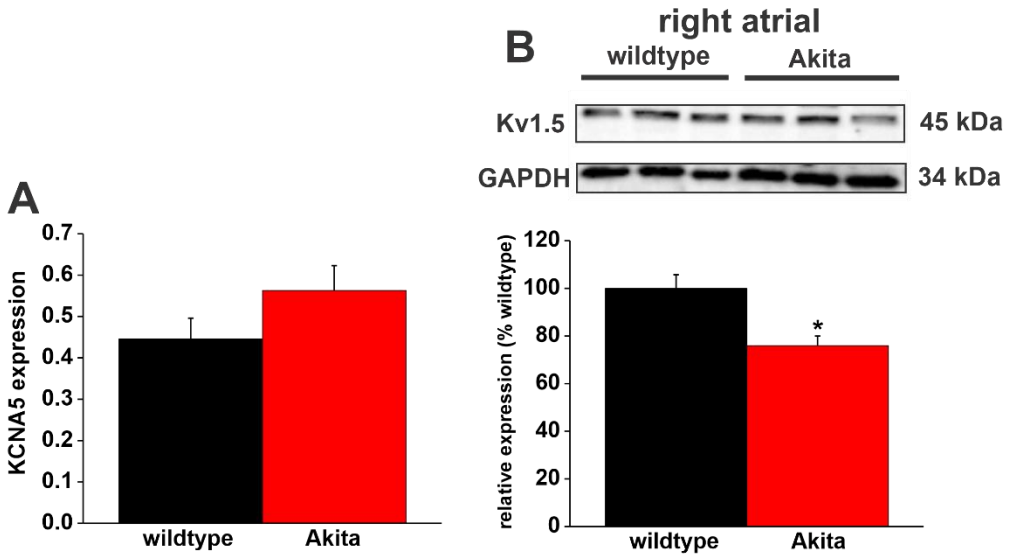

Figure S11. Atrial expression of KCNA5 gene and K_V1.5 protein in Akita mice. (*A*) Right atrial KCNA5 gene expression in wildtype and Akita mice. *P*=0.106; *n*=23 for wildtype and 15 for Akita. (*B*) Right atrial K_V1.5 expression was measured in wildtype and Akita mice. **P*<0.05 vs. wildtype by Student's *t*-test, *n*=9 for wildtype and 9 for Akita.

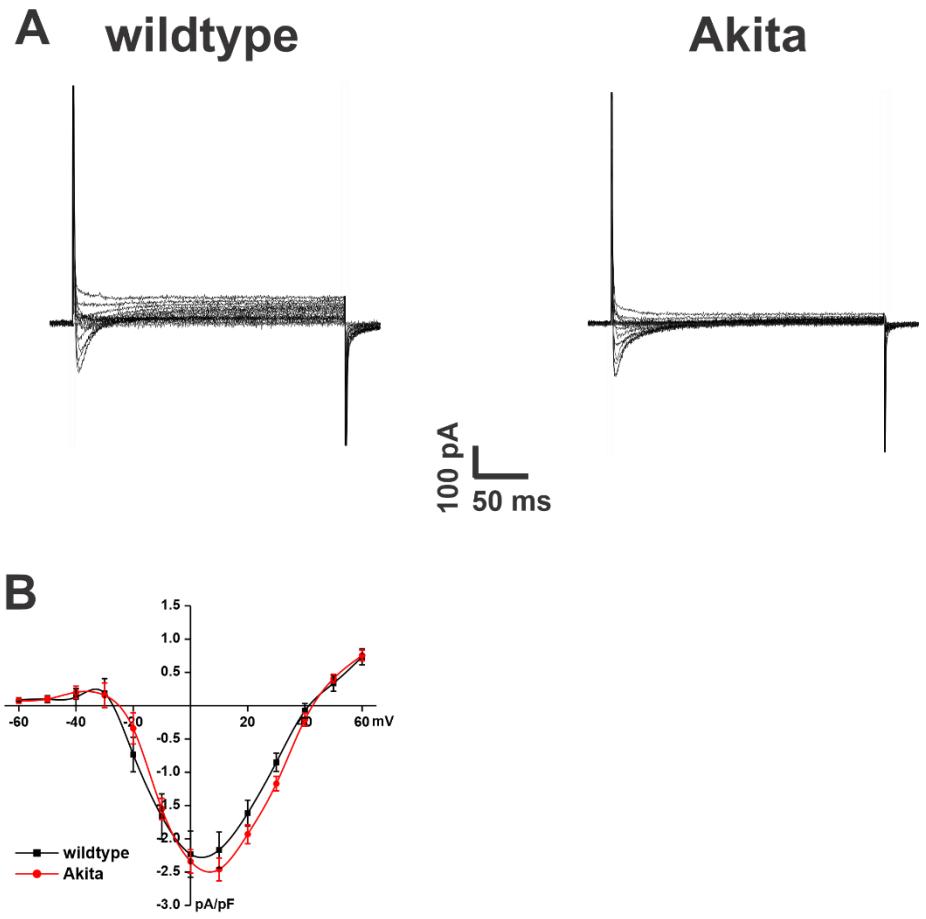

Figure S12. Measurement of atrial $I_{Ca,L}$ in Akita mice. (*A*) Representative $I_{Ca,L}$ recordings in isolated right atrial myocytes from wildtype and Akita mice. Cell capacitances for these representative recordings was 50 pF for wildtype and 41 pF for Akita. (*B*) $I_{Ca,L}$ IV curves in right atrial myocytes from wildtype and Akita mice; *n*=11 wildtype and 12 Akita right atrial myocytes. There was no difference (*P*=0.260) in $I_{Ca,L}$ between groups; data analyzed by two-way repeated measures ANOVA.

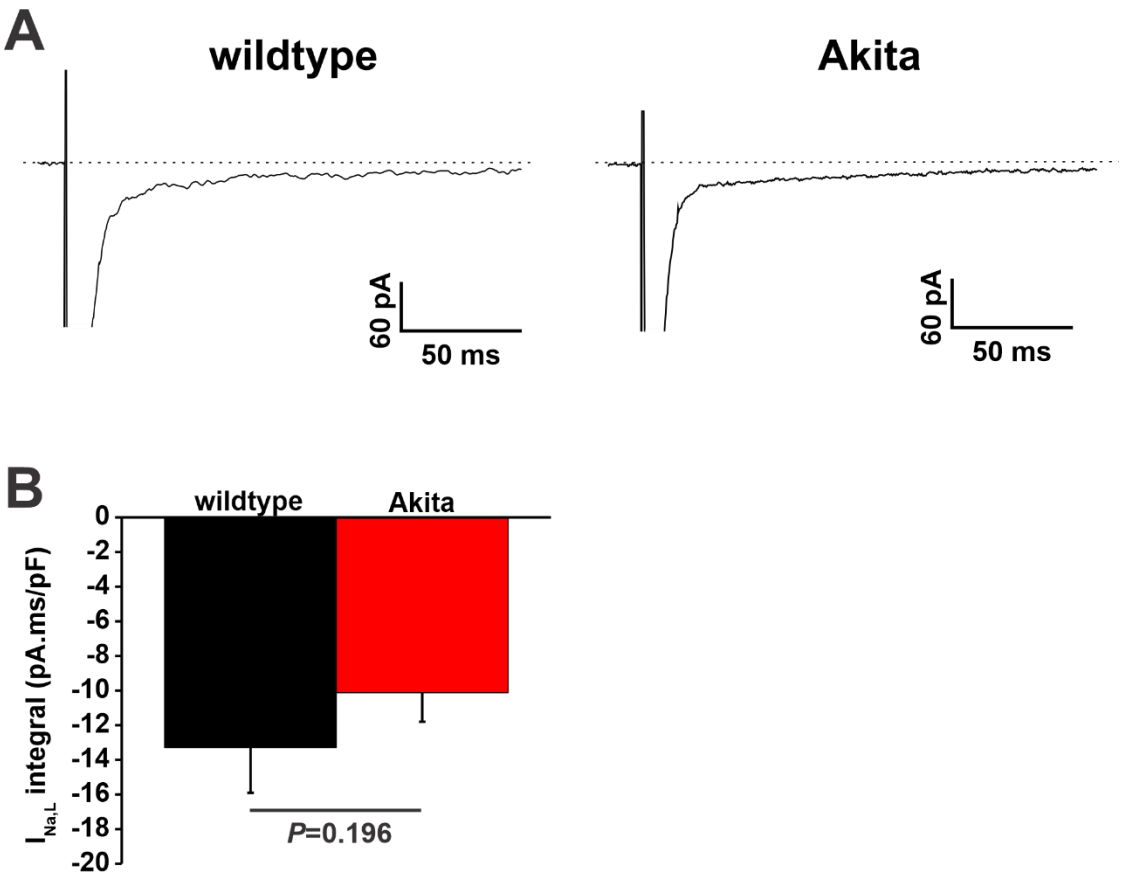

Figure S13: Late Na^+ current in Akita right atrial myocytes. (*A*) Representative $I_{Na,L}$ recordings from wildtype and Akita right atrial myocytes. Cell capacitances for these representative recordings was 38 pF for wildtype and 34 pF for Akita. (*B*) $I_{Na,L}$ (measured as an integral between 100 – 150 ms) in wildtype and Akita right atrial myocytes. Data analyzed by Student's *t*-test, *n*=10 wildtype and 9 Akita atrial myocytes.

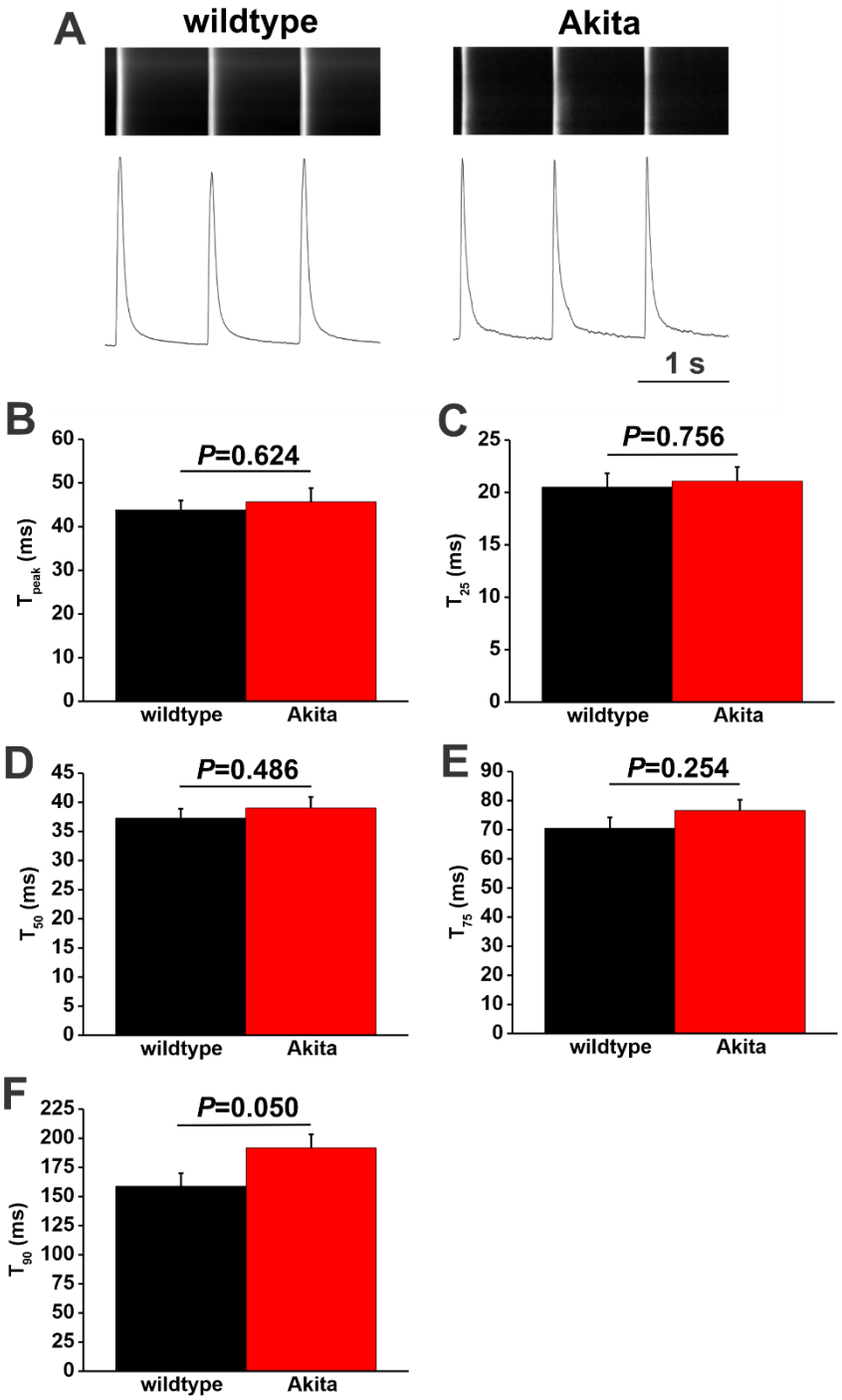

Figure S14: Calcium transient morphology in Akita atrial myocytes. (*A*) Representative confocal line scans and stimulated calcium transients in atrial myocytes from wildtype and Akita mice. (*B*) Summary of time to peak (T_{peak}) in wildtype and Akita atrial myocytes. (*C-E*) Calcium transient duration at 25% (T_{25}, panel *C*), 50% (T_{50}, panel *D*), 75% (T_{75}, panel *E*) and 90% (T_{90}, panel *E*) decay times. Data analyzed by Student's *t*-test; *n*=19 wildtype and 20 Akita atrial myocytes.

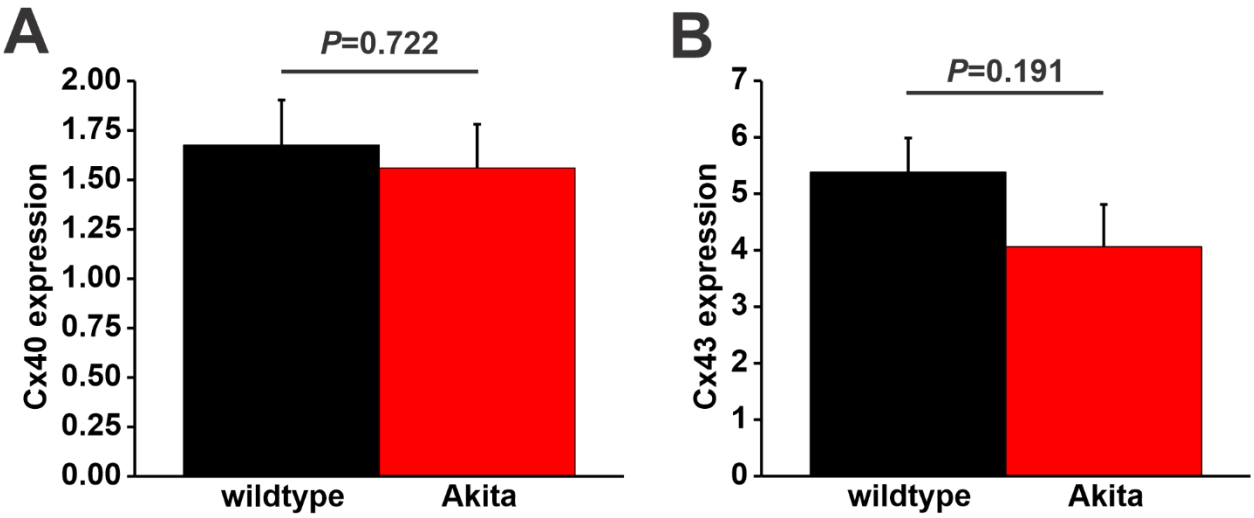

Figure S15: Expression of connexin 40 and connexin 43 in the right atrium in Akita mice. (*A*) Expression of *GJA5* (encodes Cx40) mRNA in wildtype and Akita right atria. (*B*) Expression of *GJA1* (encodes Cx43) mRNA in wildtype and Akita right atria. Data analyzed by Student's t-test; *n*=8 right atria for each group.

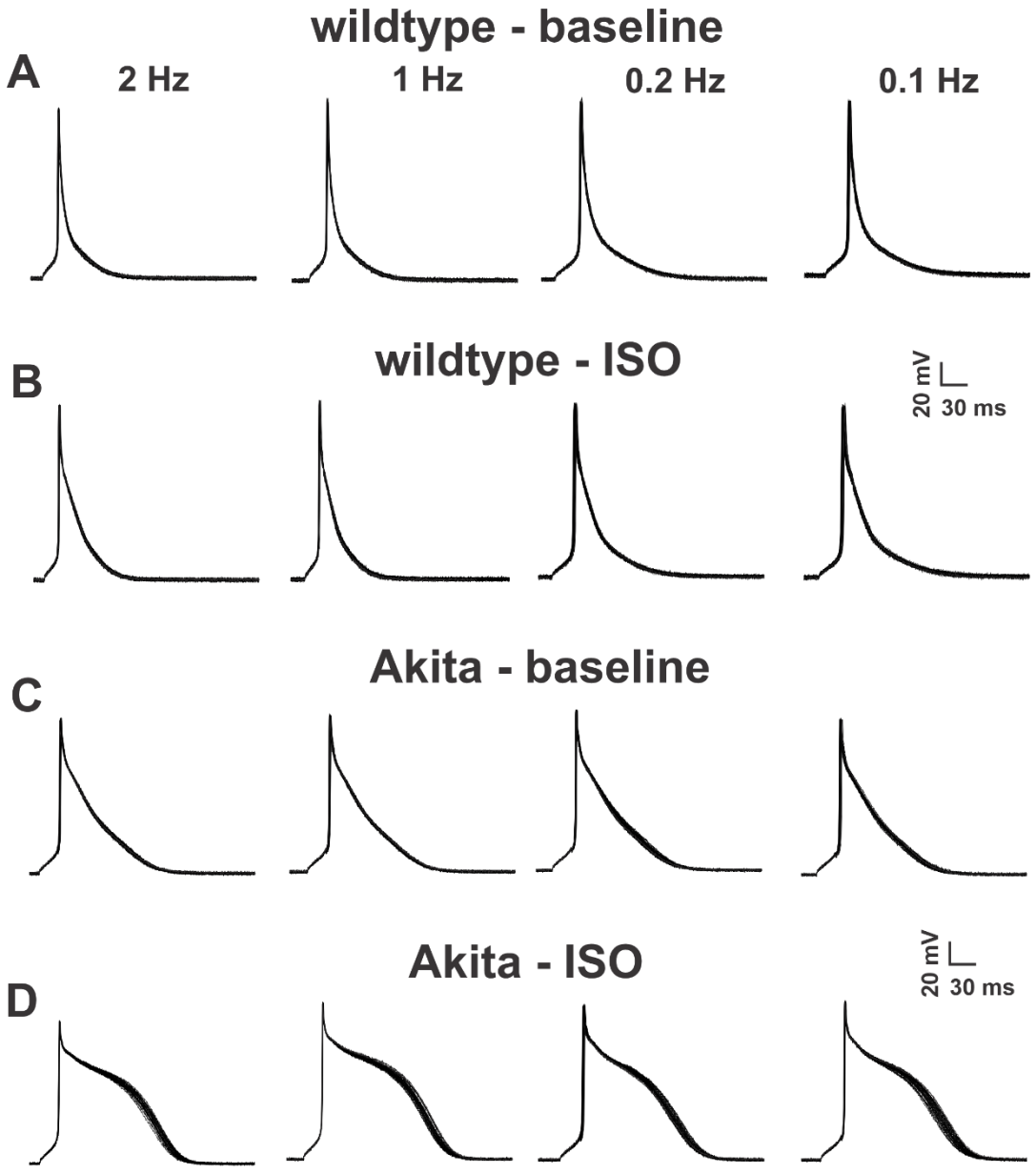

Figure S16: Assessment of early afterdepolarizations in Akita right atrial myocytes. EAD susceptibility was assessed by recording APs at pacing frequencies of 2, 1, 0.2 and 0.1 Hz in baseline conditions and in the presence of isoproterenol (ISO; 1 µM) in wildtype and Akita right atrial myocytes. Each panel contains an overlay of 30 successive APs in each condition. No EADs were observed.

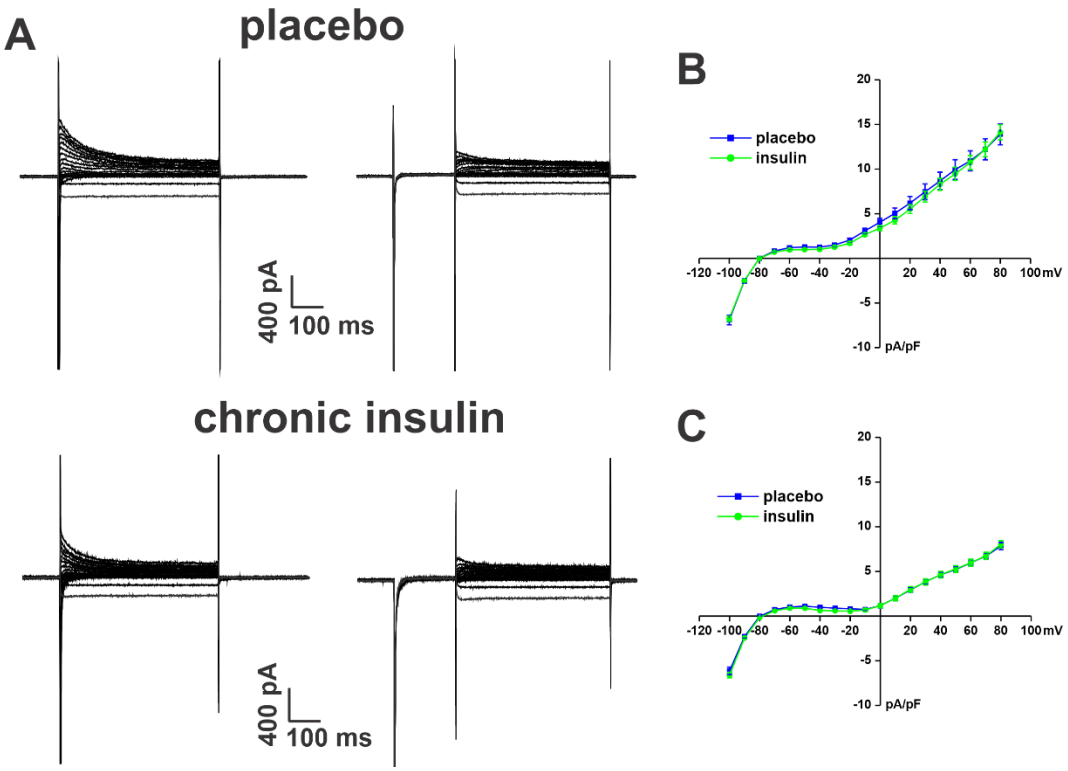

Figure S17. Chronic insulin treatment has no effect on K^+ currents in Akita mice. (*A*) Representative K^+ current recordings in right atrial myocytes from Akita mice treated chronically with insulin or placebo. The recordings on the left represent total I_K measured between -100 and +80 mV. The recordings on the right represent I_K measured between -100 and +80 mV following a pre-pulse to -40 mV to inactivate I_{to}. Cell capacitances for these representative recordings was 31 pF for wildtype and 38 pF for Akita. (*B*) I_K IV curves measured at the peak of the I_K recordings without the pre-pulse (recordings on the left in panel A) for right atrial myocytes isolated from insulin or placebo treated Akita mice. There was no difference in I_K density between groups (P=0.61 by two-way repeated measures ANOVA with Tukey's posthoc test). (*C*) I_K IV curves measured at the peak of the I_K recordings with the pre-pulse (recordings on the right in panel A) for right atrial myocytes isolated from insulin or placebo treated Akita mice. There was no difference in I_K density between groups (P=0.67 by two-way repeated measures ANOVA with Tukey's posthoc test); n=18 myocytes for placebo and 21 myocytes for chronic insulin.

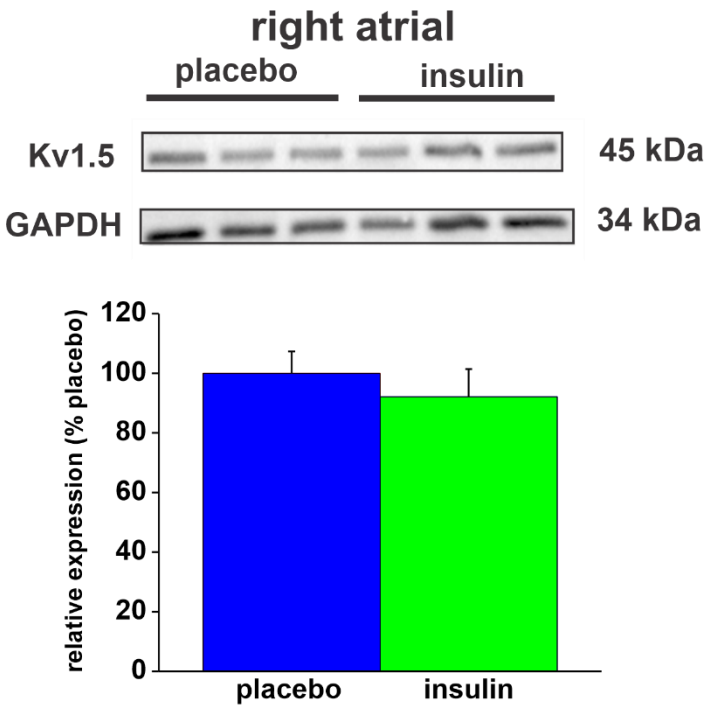

Figure S18. Protein expression of K_V1.5 in Akita mice treated chronically with insulin. Right atrial K_V1.5 was measured following chronic insulin or placebo treatment. *P*=0.56 by Student's *t*-test, *n*=12 for placebo and 12 for chronic insulin.

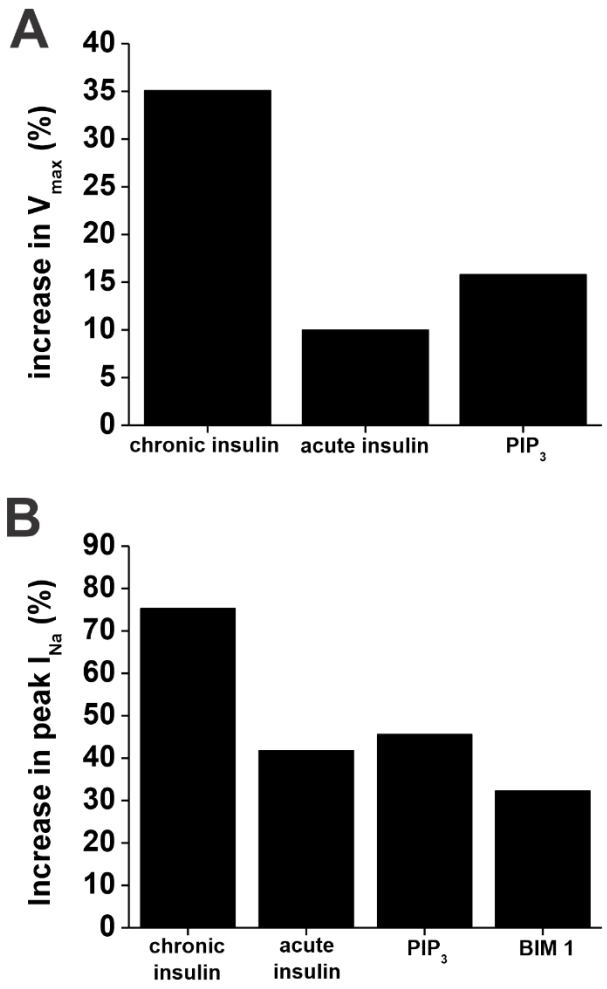

Figure S19. Comparison of the magnitude of the effects of drug treatments on AP V_{max} (*A*) and peak atrial I_{Na} (*B*) in Akita mice. Percent changes were measured relative to the specific control group for each treatment as outlined in the manuscript.

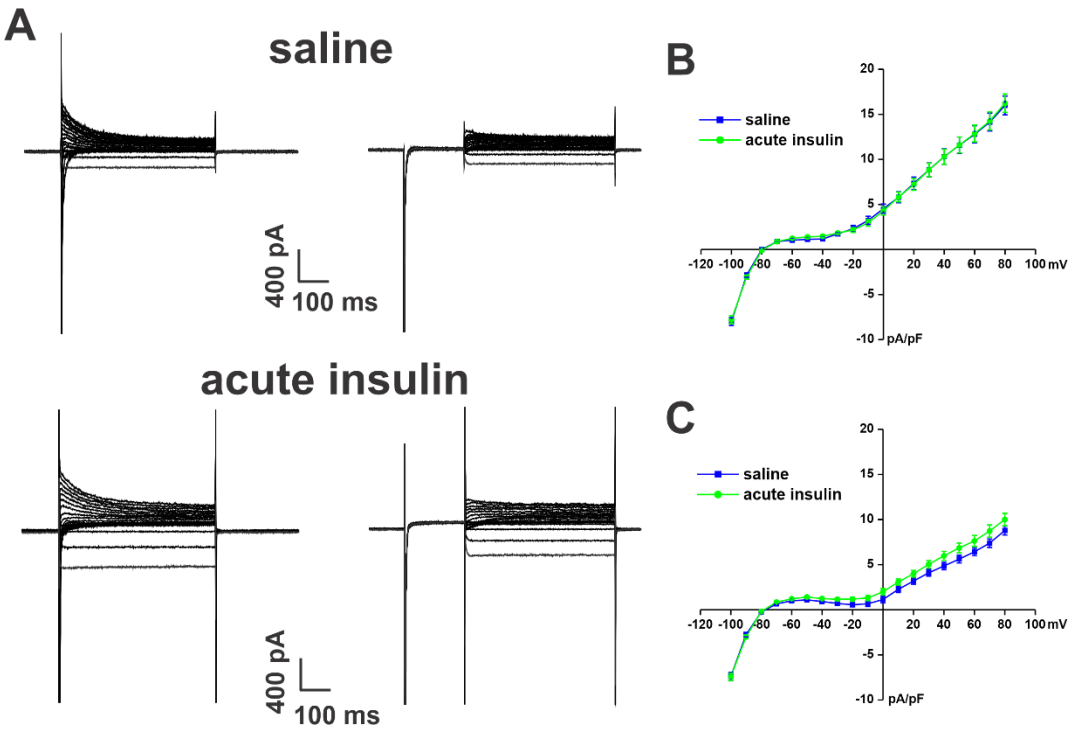

Figure S20. Acute insulin treatment has no effect on K^+ currents in Akita mice. (*A*) Representative K^+ current recordings in right atrial myocytes from Akita mice acutely injected with insulin or saline as a control. The recordings on the left represent total I_K measured between -100 and +80 mV. The recordings on the right represent I_K measured between -100 and +80 mV following a pre-pulse to -40 mV to inactivate I_{to}. Cell capacitances for these representative recordings was 35 pF for wildtype and 41 pF for Akita. (*B*) I_K IV curves measured at the peak of the I_K recordings without the pre-pulse (recordings on the left in panel *A*) for right atrial myocytes isolated from insulin or saline treated Akita mice. There was no difference in I_K density between groups (P=0.97 by two-way repeated measures ANOVA with Tukey's posthoc test). (*C*) I_K IV curves measured at the peak of the I_K recordings with the pre-pulse (recordings on the right in panel A) for right atrial myocytes isolated from insulin or saline treated Akita mice. There was no difference in I_K density between groups (P=0.08 by two-way repeated measures ANOVA with Tukey's posthoc test); n=20 myocytes for saline and 20 myocytes for acute insulin.

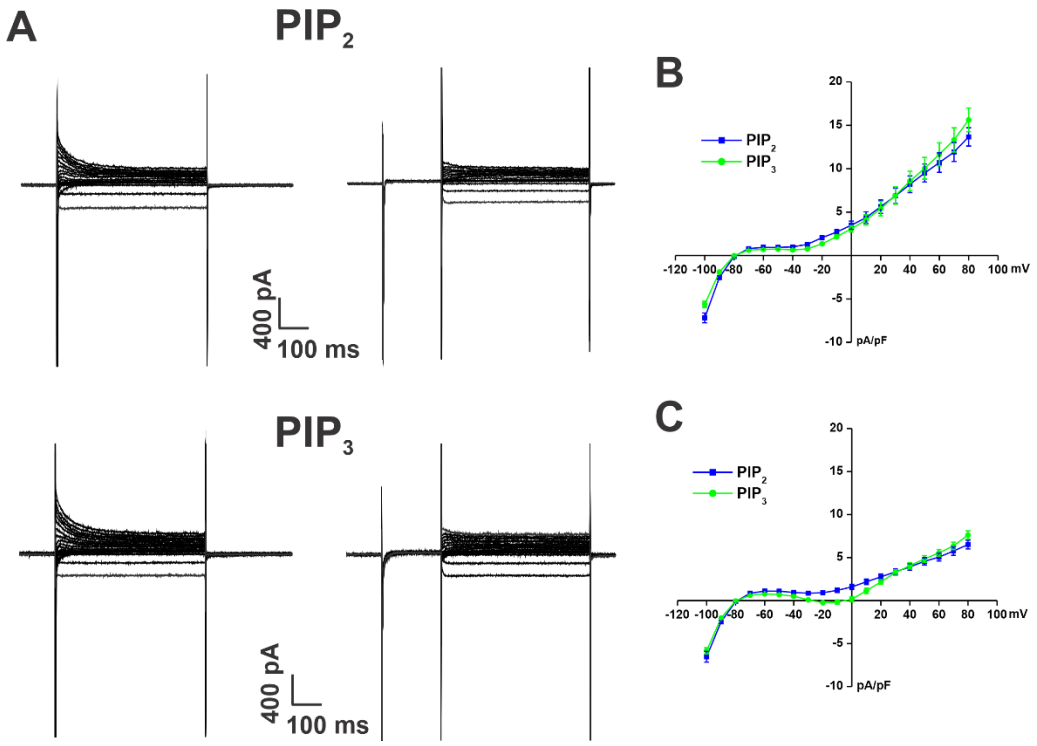

Figure S21. PIP_3 has no effect on K^+ currents in Akita mice. (*A*) Representative K^+ current recordings in right atrial myocytes from Akita mice dialyzed with PIP_3 (1 μM) or PIP_2 (1 μM). Data are from cells dialyzed for 10 min with phospholipids. The recordings on the left represent total I_K measured between -100 and +80 mV. The recordings on the right represent I_K measured between -100 and +80 mV following a pre-pulse to -40 mV to inactivate I_{to}. Cell capacitances for these representative recordings was 44 pF for wildtype and 52 pF for Akita. (*B*) I_K IV curves measured at the peak of the I_K recordings without the pre-pulse (recordings on the left in panel *A*) for Akita right atrial myocytes dialyzed with PIP_3 or PIP_2. There was no difference in I_K density between groups (P=0.76 by two-way repeated measures ANOVA with Tukey's posthoc test). (*C*) I_K IV curves measured at the peak of the I_K recordings with the pre-pulse (recordings on the right in panel A) for Akita right atrial myocytes dialyzed with PIP_3 or PIP_2. There was no difference in I_K density between groups (P=0.39 by two-way repeated measures ANOVA with Tukey's posthoc test); n=9 myocytes for PIP_2 and 10 myocytes for PIP_3.

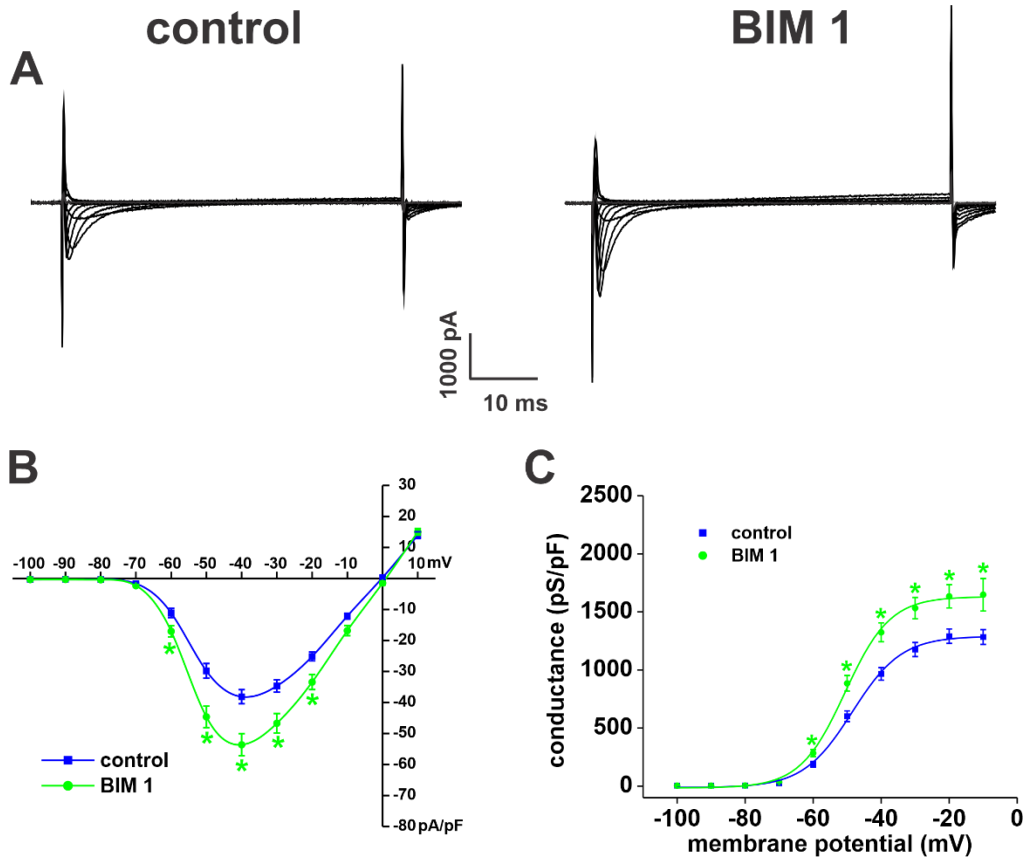

Figure S22. Effects of protein kinase C inhibition in I_{Na} in Akita mice. (*A*) Representative I_{Na} recordings in right atrial myocytes from Akita mice following dialysis with the PKC inhibitor BIM 1 (1 μM) compared to control Akita myocytes. Cell capacitances for these representative recordings was 34 pF for wildtype and 39 pF for Akita. (*B*) I_{Na} IV curves for right atrial myocytes from untreated Akita mice in control conditions and after dialysis with BIM 1. (C) I_{Na} activation curves for right atrial myocytes from Akita mice in control conditions and after dialysis with BIM 1. For panels *B* and *C* **P*<0.05 vs. control by two-way repeated measures ANOVA with Tukey's posthoc test; *n*=18 myocytes for control and 20 myocytes for BIM 1. Refer to Supplemental Table 13 for additional analysis of I_{Na} activation kinetics.

Table S1: Duration of arrhythmia in wildtype and Akita mice that were induced into atrial fibrillation

	wildtype	Akita
< 5s	100% (2/2)	15% (2/13)
5-30 s	0% (0/2)	62% (8/13)
>30 s	0% (0/2)	23% (3/13)

Numbers in parentheses indicate the number of mice in each group.

Table S2: Duration of arrhythmia in wildtype mice treated with STZ that were induced into atrial fibrillation

	veh	STZ
< 5s	100% (3/3)	37.5% (3/8)
5-30 s	0% (0/3)	37.5% (3/8)
>30 s	0% (0/3)	25% (2/8)

Numbers in parentheses indicate the number of mice in each group. veh, vehicle; STZ, streptozotocin.

Table S3: Duration of arrhythmia in Akita mice treated chronically with insulin or placebo that were induced into atrial fibrillation

	Placebo	chronic insulin
< 5s	54% (7/13)	83% (5/6)
5-30 s	38% (5/13)	17% (1/6)
>30 s	8% (1/13)	0% (0/6)

Mice were treated with insulin (or placebo) for 4 weeks prior to investigation. Numbers in parentheses indicate the number of mice in each group.

Table S4: Duration of arrhythmia in Akita mice treated acutely with insulin or saline that were induced into atrial fibrillation

	Saline	acute insulin
< 5s	17% (1/6)	20% (1/5)
5-30 s	67% (4/6)	60% (3/5)
>30 s	17% (1/6)	20% (1/5)

Mice were treated acutely with insulin (or saline) immediately prior to investigation. Numbers in parentheses indicate the number of mice in each group.

Table S5: ECG intervals in wildtype and Akita mice

	Wildtype	Akita	*P* value
Heart rate (beats/min)	556 ± 21	496 ± 13*	0.022
R-R interval (ms)	108.7 ± 3.7	121.7 ± 3.4*	0.024
P wave (ms)	26.7 ± 1.0	38.1 ± 1.3*	<0.001
P-R interval (ms)	46.3 ± 1.7	54.7 ± 1.6*	0.003

Data are means ± SEM; *n* = 7-10 mice per group. *P<0.05 vs. wildtype by Student's *t*-test.

Table S6: ECG intervals in wildtype mice treated with STZ

	veh	STZ	*P* value
Heart rate (beats/min)	520 ± 9	508 ± 14	0.566
R-R interval (ms)	116.1 ± 2.2	120.0 ± 3.8	0.375
P wave (ms)	25.3 ± 0.5	27.7 ± 0.7*	0.010
P-R interval (ms)	45.1 ± 0.8	49.0 ± 1.5	0.069

Data are means ± SEM; *n* = 17-19 mice per group. *P<0.05 vs. wildtype by Student's *t*-test.

Table S7: ECG intervals in placebo and chronic insulin treated Akita mice

	placebo	chronic insulin	*P* value
Heart rate (beats/min)	501 ± 10	544 ± 11*	0.007
R-R interval (ms)	120.9 ± 2.9	111.3 ± 2.4*	0.005
P wave (ms)	33.0 ± 1.3	28.7 ± 1.0*	0.023
P-R interval (ms)	55.8 ± 2.2	51.4 ± 1.7	0.07

Mice were treated with insulin (or placebo) for 4 weeks prior to investigation. Data are means ± SEM; *n*=21-22 mice per group. *P<0.05 vs. placebo by Student's *t*-test.

Table S8: ECG intervals in saline and acute insulin treated Akita mice

	saline	acute insulin	*P* value
Heart rate (beats/min)	507 ± 28	499 ± 9	0.32
R-R interval (ms)	121.3 ± 8.7	120.6 ± 2.3	0.32
P wave (ms)	38.7 ± 0.71	36.2 ± 0.8*	0.03
P-R interval (ms)	57.0 ± 1.8	56.9 ± 2.3	0.95

Mice were treated acutely with insulin (or saline) immediately prior to investigation. Data are means ± SEM; *n*=7-8 mice per group. *P<0.05 vs. saline by Student's *t*-test.

Table S9: Echocardiographic measurements in wildtype and Akita mice

	Wildtype	Akita	*P* value
LVAWd (mm)	0.89 ± 0.02	0.79 ± 0.05*	0.024
LVPWd (mm)	0.87 ± 0.02	0.82 ± 0.03	0.576
LVIDd (mm)	4.72 ± 0.12	4.32 ± 0.08*	0.003
LVAWs (mm)	1.35 ± 0.04	1.24 ± 0.06	0.056
LVPWs (mm)	1.19 ± 0.02	1.16 ± 0.04	0.768
LVIDs (mm)	3.42 ± 0.12	3.00 ± 0.09*	0.011
EF (%)	53.39 ± 2.1	58.08 ± 1.7	0.182
LA $area_{max}$ (mm^2)	6.51 ± 0.3	7.36 ± 0.5*	0.042
LA $area_{min}$ (mm^2)	4.20 ± 0.3	4.63 ± 0.4	0.320
RA $area_{max}$ (mm^2)	5.55 ± 0.3	6.02 ± 0.4	0.294
RA $area_{min}$ (mm^2)	3.27 ± 0.22	4.21 ± 0.7	0.310

LVAW, left ventricular anterior wall thickness; LVPW, left ventricular posterior wall thickness; LVID, left ventricular internal diameter. LVAW, LVPW and LVID measurements were made during systole (s) and diastole (d). EF, ejection fraction; LA $area_{max}$, maximum left atrial area; LA $area_{min}$, minimum left atrial area. RA $area_{max}$, maximum right atrial area; RA $area_{min}$, minimum right atrial area. Data are means ± SEM; *n* = 11 mice per group. **P*<0.05 vs. wildtype by Student's *t*-test.

Table S10: Action potential parameters in right atrial myocytes from wildtype and Akita mice

	wildtype	Akita	*P* value
RMP (mV)	-78.2 ± 0.2	-77.7 ± 0.3	0.116
V_{max} (V/s)	172.9 ± 6.0	135.7 ± 6.9*	<0.001
OS (mV)	57.5 ± 2.3	46.2 ± 2.5*	0.002
APD_{50} (ms)	9.7 ± 1.3	14.3 ± 1.5*	0.022
APD_{70} (ms)	19.5 ± 2.4	26.4 ± 2.7*	0.044
APD_{90} (ms)	41.3 ± 3.2	51.3 ± 3.6*	0.047

RMP, resting membrane potential; V_{max}, AP upstroke velocity; OS, overshoot; APD_{50}, AP duration at 50% repolarization; APD_{70}, AP duration at 70% repolarization; APD_{90}, AP duration at 90% repolarization. **P*<0.05 vs wildtype by Student's *t*-test; *n*=18 wildtype and 16 Akita myocytes.

Table S11: Action potential parameters in left atrial myocytes from wildtype and Akita mice

	wildtype	Akita	*P* value
RMP (mV)	-78.0 ± 0.3	-77.8 ± 0.3	0.634
V_{max} (V/s)	168.1 ± 6.6	141.2 ± 5.8*	0.036
OS (mV)	53.8 ± 3.0	43.6 ± 5.8*	0.009
APD_{50} (ms)	9.1 ± 0.8	16.4 ± 1.3*	<0.001
APD_{70} (ms)	17.0 ± 1.4	29.7 ± 2.3*	<0.001
APD_{90} (ms)	36.4 ± 2.6	55.5 ± 4.5*	0.001

RMP, resting membrane potential; V_{max}, AP upstroke velocity; OS, overshoot; APD_{50}, AP duration at 50% repolarization; APD_{70}, AP duration at 70% repolarization; APD_{90}, AP duration at 90% repolarization. **P*<0.05 vs wildtype by Student's *t*-test; *n*=12 wildtype and 11 Akita myocytes.

Table S12: Action potential parameters in ventricular myocytes from wildtype and Akita mice

	wildtype	Akita	*P* value
RMP (mV)	-80.4 ± 0.4	-80.7 ± 0.3	0.663
V_{max} (V/s)	185.4 ± 7.3	177.3 ± 9.6	0.540
OS (mV)	60.4 ± 3.1	67.9 ± 2.2	0.08
APD_{50} (ms)	2.7 ± 0.1	4.7 ± 0.9*	0.04
APD_{70} (ms)	5.0 ± 0.3	9.1 ± 1.9*	0.04
APD_{90} (ms)	15.0 ± 1.1	22.5 ± 3.2*	0.03

RMP, resting membrane potential; V_{max}, AP upstroke velocity; OS, overshoot; APD_{50}, AP duration at 50% repolarization; APD_{70}, AP duration at 70% repolarization; APD_{90}, AP duration at 90% repolarization. **P*<0.05 vs wildtype by Student's *t*-test; *n*=8 wildtype and 11 Akita ventricular myocytes.

Table S13: I_{Na} kinetics

	G_{max} (pS/pF)	P value	$V_{1/2(act)}$ (mV)	P value	k (mV)	P value
Wildtype right atrial	1973.2 ± 74.3	<0.001	-51.5 ± 0.6	0.009	5.1 ± 0.1	<0.001
Akita right atrial	1232.9 ± 85.9*		-48.9 ± 0.7*		6.2 ± 0.2*	
Wildtype left atrial	2095.5 ± 300.1	0.009	-52.4 ± 1.5	<0.05	5.7 ± 0.4	0.82
Akita left atrial	1412.0 ± 79.1*		-49.7 ± 1.2*		5.8 ± 0.3	
Akita placebo	927.1 ± 86.9	<0.001	-47.7 ± 0.8	0.71	4.4 ± 0.2	0.78
Akita insulin (chronic)	1589.5 ± 134.1*		-48.2 ± 1.2		4.3 ± 0.5	
Akita saline	1214.1 ± 37.8	0.01	-49.7 ± 1.2	0.86	6.1 ± 0.3	0.11
Akita insulin (acute)	1535. 5 ± 60.3*		-51.0 ± 0.6		5.6 + 0.2	
Akita PIP_2	863.0 ± 98.8	<0.001	-48.8 ± 0.9	0.61	5.6 ± 0.3	0.58
Akita PIP_3	1359.3 ± 79.1*		-48.9 ± 0.7		5.8 ± 0.2	
Akita control	1252.5 ± 60.8	0.02	-48.9 ± 0.8	0.006	6.2 ± 0.1	0.07
Akita BIM1	1543.5 ± 96.9*		-51.4 ± 0.5*		5.6 ± 0.1	

G_{max}, maximum conductance, $V_{1/2(act)}$, voltage at which 50% of channels are activated; k, slope factor. **P*<0.05 vs control value as indicated in the table cell immediately above, *n* values are as reported in figure legends for each experimental group in the main manuscript. Data analyzed by Student's *t*-test.

Table S14: Action potential parameters in right atrial myocytes from Akita mice treated chronically with insulin

	placebo	chronic insulin	*P* value
RMP (mV)	-78.1 ± 0.2	-78.9 ± 0.1*	0.002
V_{max} (V/s)	126.4 ± 4.4	170.8 ± 2.7*	<0.001
OS (mV)	46.6 ± 2.6	56.3 ± 1.2*	<0.001
APD_{50} (ms)	18.8 ± 3.4	18.7 ± 2.0	0.560
APD_{70} (ms)	33.1 ± 5.5	35.1 ± 2.9	0.733
APD_{90} (ms)	61.5 ± 8.0	67.2 ± 4.6	0.518

RMP, resting membrane potential; V_{max}, AP upstroke velocity; OS, overshoot; APD_{50}, AP duration at 50% repolarization; APD_{70}, AP duration at 70% repolarization; APD_{90}, AP duration at 90% repolarization. *P<0.05 vs placebo by Student's t-test; n=19 placebo and 14 insulin treated myocytes.

Table S15: Action potential parameters in right atrial myocytes from Akita mice treated acutely with insulin

	saline	acute insulin	*P* value
RMP (mV)	-77.7 ± 0.4	-77.7 ± 0.3	0.567
V_{max} (V/s)	137.4 ± 4.1	151.2 ± 5.2*	0.03
OS (mV)	49.3 ± 1.9	49.0 ± 1.7	0.607
APD_{50} (ms)	14.6 ± 1.0	16.5 ± 2.8	0.766
APD_{70} (ms)	28.6 ± 2.0	29.7 ± 4.4	0.620
APD_{90} (ms)	58.3 ± 3.6	53.3 ± 5.5	0.423

RMP, resting membrane potential; V_{max}, AP upstroke velocity; OS, overshoot; APD_{50}, AP duration at 50% repolarization; APD_{70}, AP duration at 70% repolarization; APD_{90}, AP duration at 90% repolarization. *P<0.05 vs saline by Student's t-test; n=14 saline and 18 insulin treated myocytes.

Table S16: Action potential parameters in right atrial myocytes from Akita mice treated PIP_3

	PIP_2	PIP_3	*P* value
RMP (mV)	-78.3 ± 0.2	-79.2 ± 0.2*	0.015
V_{max} (V/s)	138.5 ± 6.8	160.4 ± 9.5*	0.039
OS (mV)	53.5 ± 3.4	48.9 ± 2.6	0.286
APD_{50} (ms)	12.4 ± 1.8	13.0 ± 2.0	0.194
APD_{70} (ms)	26.5 ± 3.3	27.5 ± 4.1	0.194
APD_{90} (ms)	56.9 ± 4.9	64.2 ± 6.2	0.052

RMP, resting membrane potential; V_{max}, AP upstroke velocity; OS, overshoot; APD_{50}, AP duration at 50% repolarization; APD_{70}, AP duration at 70% repolarization; APD_{90}, AP duration at 90% repolarization. *P<0.05 vs PIP_2 by Student's t-test; n=7 PIP_2 and 8 PIP_3 treated myocytes.

Supplemental Table 17: Quantitative PCR primers

Gene	Gene product	Primer Sequence (5'→ 3')	Amplicon length (bp)
SCN5a	$Na_v1.5$	Forward: GGAGTACGCCGACAAGATGT Reverse: ATCTCGGCAAAGCCTAAGGT	171
KCNA5	$K_v1.5$	Forward: TTATTCTTATGGCTGACGAGTGC Reverse: AAGGCACCAATAGTACATCCCAG	204
GJA5	Cx40	Forward: CACAGTCATCGGCAAGGTCT Reverse: ATGGTATCGCACCGGAAGTC	117
GJA1	Cx43	Forward: CCAAGGAGTTCCACCACTTTG Reverse: CCATGTCTGGGCACCTCTCT	70
GAPDH	GAPDH	Forward: AATGGGGTGAGGCCGGTGCT Reverse: CACCCTTCAAGTGGGCCCCG	87

References

1. Yoshioka M, Kayo T, Ikeda T, Koizumi A, A novel locus, Mody4, distal to D7Mit189 on chromosome 7 determines early-onset NIDDM in nonobese C57BL/6 (Akita) mutant mice. *Diabetes.* **46,** 887-894 (1997).
2. Krishnaswamy PS*, et al.*, Altered parasympathetic nervous system regulation of the sinoatrial node in Akita diabetic mice. *J Mol Cell Cardiol.* **82,** 125-135 (2015).
3. Bugger H*, et al.*, Type 1 diabetic akita mouse hearts are insulin sensitive but manifest structurally abnormal mitochondria that remain coupled despite increased uncoupling protein 3. *Diabetes.* **57,** 2924-2932 (2008).
4. Hsueh W*, et al.*, Recipes for creating animal models of diabetic cardiovascular disease. *Circ Res.* **100,** 1415-1427 (2007).
5. Bugger H*, et al.*, Genetic loss of insulin receptors worsens cardiac efficiency in diabetes. *J Mol Cell Cardiol.* **52,** 1019-1026 (2012).
6. Egom EE*, et al.*, Impaired sinoatrial node function and increased susceptibility to atrial fibrillation in mice lacking natriuretic peptide receptor C. *J Physiol.* **593,** 1127-1146 (2015).
7. Jansen HJ*, et al.*, Atrial structure, function and arrhythmogenesis in aged and frail mice. *Sci Rep.* **7,** 44336 (2017).
8. Azer J, Hua R, Krishnaswamy PS, Rose RA, Effects of natriuretic peptides on electrical conduction in the sinoatrial node and atrial myocardium of the heart. *J Physiol.* **592,** 1025-1045 (2014).
9. Nygren A, Lomax AE, Giles WR, Heterogeneity of action potential durations in isolated mouse left and right atria recorded using voltage-sensitive dye mapping. *Am J Physiol Heart Circ Physiol.* **287,** H2634-2643 (2004).
10. Glukhov AV*, et al.*, Functional anatomy of the murine sinus node: high-resolution optical mapping of ankyrin-B heterozygous mice. *Am J Physiol Heart Circ Physiol.* **299,** H482-491 (2010).
11. Fedorov VV*, et al.*, Application of blebbistatin as an excitation-contraction uncoupler for electrophysiologic study of rat and rabbit hearts. *Heart Rhythm.* **4,** 619-626 (2007).
12. Farman GP*, et al.*, Blebbistatin: use as inhibitor of muscle contraction. *Pflugers Arch.* **455,** 995-1005 (2008).
13. Morley GE*, et al.*, Characterization of conduction in the ventricles of normal and heterozygous Cx43 knockout mice using optical mapping. *J Cardiovasc Electrophysiol.* **10,** 1361-1375 (1999).
14. Springer J*, et al.*, The natriuretic peptides BNP and CNP increase heart rate and electrical conduction by stimulating ionic currents in the sinoatrial node and atrial myocardium following activation of guanylyl cyclase-linked natriuretic peptide receptors. *J Mol Cell Cardiol.* **52,** 1122-1134 (2012).
15. Hua R*, et al.*, Distinct patterns of constitutive phosphodiesterase activity in mouse sinoatrial node and atrial myocardium. *PLoS One.* **7,** e47652 (2012).
16. Lomax AE, Kondo CS, Giles WR, Comparison of time- and voltage-dependent K+ currents in myocytes from left and right atria of adult mice. *Am J Physiol Heart Circ Physiol.* **285,** H1837-1848 (2003).
17. Kuo HC*, et al.*, A defect in the Kv channel-interacting protein 2 (KChIP2) gene leads to a complete loss of I(to) and confers susceptibility to ventricular tachycardia. *Cell.* **107,** 801-813 (2001).
18. Fiset C, Clark RB, Larsen TS, Giles WR, A rapidly activating sustained K+ current modulates repolarization and excitation-contraction coupling in adult mouse ventricle. *J Physiol.* **504 (Pt 3),** 557-563 (1997).

19. Mangoni ME*, et al.*, Functional role of L-type Cav1.3 Ca2+ channels in cardiac pacemaker activity. *Proc Natl Acad Sci U S A.* **100,** 5543-5548 (2003).
20. Zhang Z*, et al.*, Functional roles of Cav1.3(alpha1D) calcium channels in atria: insights gained from gene-targeted null mutant mice. *Circulation.* **112,** 1936-1944 (2005).